Physics – Uspekhi **40** (7) 717 – 737 (1997)

REVIEWS OF TOPICAL PROBLEMS PACS numbers: **61.46 + w**, **68.70. + w**, **85.42. + m**

Formation and growth of carbon nanostructures: fullerenes, nanoparticles, nanotubes and cones

Yu E Lozovik, A M Popov

Contents

1. Introduction **717**
2. Models of fullerene formation **718**
2.1 Fabrication and structure of fullerenes; 2.2 Fullerene assemblage from graphite fragments; 2.3 'Nautilus' model; 2.4 Assemblage from clusters; 2.5 'Fullerene road'; 2.6 Annealing of carbon clusters; 2.7 Crystallization of a liquid cluster into a fullerene
3. Magic fullerenes and fullerene isomers **724**
3.1 Set of magic fullerenes; 3.2 Role of fullerene transformations; 3.3 Energetics and structure of magic fullerenes; 3.4 Formation of fullerene isomers; 3.5 Role of the buffer gas
4. Mechanisms of carbon nanoparticle formation **727**
4.1 Shell structure of nanoparticles and the 'nautilus' model; 4.2 Simulation of shell-by-shell growth; 4.3 Crystallization of a liquid cluster; 4.4 Formation of nanoparticles with metal or metal carbide cores; 4.5 Formation of nanoparticle chains
5. Mechanisms for the growth of nanotubes and cones **730**
5.1 Growth of multishell nanotubes with the help of catalysts; 5.2 Production and structure of nanotubes; 5.3 Mechanisms for the growth of multishell nanotubes; 5.4 Mechanisms for the growth of single-shell nanotubes; 5.5 Nuclei for the growth of nanotubes; 5.6 Growth of single-shell nanotubes with the help of catalysts; 5.7 Formation of nanotube bundles; 5.8 Formation of carbon cones
6. Mechanisms for the formation and production of clusters and cluster materials **734**
6.1 Production of large magic fullerenes; 6.2 Production of nanotubes with metal cores; 6.3 Production of a crystal from single-shell nanotubes
7. Conclusions **735**
References **735**

Abstract. Various formation models for fullerenes and other carbon nanostructures are reviewed. The formation models considered include fullerene assembling from graphite sheets, 'nautilus' model, assemblage from clusters, 'fullerene road', and carbon cluster annealing. The selection of magic fullerenes and fullerene isomers is discussed. Carbon nanoparticle formation mechanisms are analyzed and their relation to fullerene formation mechanisms is outlined. Molecular dynamics simulation of the possible mechanisms of nanoparticle formation is considered and possible growth nuclei and growth mechanisms for single- and multishell nanotubes and for carbon cones are discussed. Some promising techniques intended for fabrication of carbon-containing nanoobjects were described.

Yu E Lozovik, A M Popov Institute of Spectroscopy,
Russian Academy of Sciences
142092 Troitsk, Moscow region, Russia
E-mail: lozovik@isan.msk.su

Received 6 November 1996, revised 21 March 1997
Uspekhi Fizicheskikh Nauk **167** (7) 751 – 774 (1997)
Translated by G N Chuev; edited by A Radzig

"*The onion coats are so harmonic*
To comfort and to joy the Master.
A larger ring around smaller ring
Concealing other rings
More delicate and very thin,
Reiterated as echo symphonic
And generated as a perfect cluster."
(V Shimborskya†)

1. Introduction

The experimental detection of a stable cluster C_{60} with icosahedral symmetry [1] and a large variety of other fullerenes (see, for example, reviews [2 – 4]) in successive years can be ranked among the most brilliant discoveries of the last decade. Curl, Kroto, and Smalley were awarded the 1996 Nobel prize in Chemistry for this outstanding finding. The surprising thing is that a crucially new carbon state was only found after centuries of use of various forms of the substance, to say nothing of the comprehensive study of the well-known crystal forms of carbon, like graphite and diamond. Curiously, quantum chemical calculations predicted the existence of C_{60} more than decade before [6]. We shall not discuss the history of C_{60} discovery here but concentrate on the question

† V Shimborskya — 1996 Nobel prize winner in literature.

of the mechanism for the formation of this complicated and symmetric cluster in real experimental conditions. It can be alternatively reformulated with emphasis on more applied aspects of the problem. Let us assume that according to calculations a complicated cluster (or complicated molecule) may exist. What could be a possible mechanism for its formation? What are the optimum conditions for its production? The adequacy of raising these questions is by no means apparent if we refer them to complicated biological molecules like nucleic acids. Or in other words, what is the limit of *molecular design*? These questions are particularly acute nowadays in connection with the possibility of producing various cluster materials and nanostructures. In this review we have restricted ourselves to the discussion of possible mechanisms for the formation of fullerenes and other carbon nanostructures such as nanopart-icles, nanotubes, and cones. Although a commonly accepted scheme for the formation of a carbon nanostructure is still lacking and the models discussed are only hypothetical, experimental and theoretical data accumulated in this actual field need systematization and critical comprehension.

2. Models of fullerene formation

2.1 Fabrication and structure of fullerenes

Fullerenes were discovered through the interpretation of the following experimental fact: in a mass-spectrum measured under certain ablation conditions the peak corresponding to C_{60} was 40-fold higher than the peaks corresponding to other clusters [1]. To explain this phenomenon, the authors of [1] assumed the existence of a stable cluster C_{60} in the form of a truncated icosahedron in which all atoms lay on a sphere in the vertices of 12 regular pentagons and 20 hexagons. This cluster was referred to as a fullerene. Apart from the fullerene C_{60}, the experiments revealed at a time some other carbon clusters with a similar structure consisting of tens of atoms lying on a spherical surface in the vertices of pentagons and hexagons. One of the main criteria for the adequacy of a model for fullerene formation is its capacity to explain the greater abundance of fullerene C_{60} relative to other fullerenes. An important breakthrough was the production of the fullerene C_{60} in macroscopic quantities by the evaporation of graphite electrodes in an arc discharge [5]. Subsequently, some other methods of fullerene production were proposed and a number of experiments were carried out to examine the conditions and processes of fullerene formation. As new experimental facts were revealed, new models of fullerene formation were proposed to explain them. However, the question is still to be clarified. In this section we analyze the models for fullerene formation dealing mainly with the assemblage of fullerenes in carbon plasma and leaving aside alternative possibilities for their formation (such as reactions between hydrocarbons, for example).

2.2 Fullerene assemblage from graphite fragments

The fullerene C_{60} was initially assumed to be assembled from plane sheets broken away from the graphite layer under ablation [7]. The simplest assemblage is the joining of six clusters of C_{10} consisting of twin hexagons [2, 3]. Another possibility [2, 3] is the curling of graphite sheets into cups making up the two halves of the fullerene C_{60} (Fig. 1), which subsequently join with smaller graphite fragments to form C_{60}. According to this elegant model, the presence of optimal

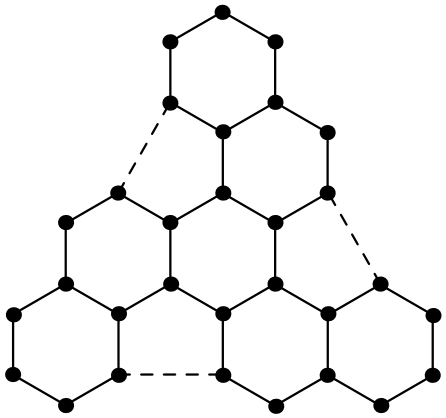

Figure 1. The plane sheet curled into the cup which makes up a half of fullerene C_{60} [3]. The bonds formed during the process are shown by the dashed lines.

conditions for C_{60} formation with a large yield is explained by the fact that just these fragments are the main products of graphite evaporation under conditions involved. However, the model fails to explain the following facts:

(1) Soot obtained as a result of graphite evaporation under optimal conditions contains up to 13% of C_{60} [8]. Hence, according to the model at hand, a significant part of the evaporated graphite must be sheets of a special shape, which seems unlikely;

(2) Fullerene C_{60} is formed not only as a result of graphite evaporation but also upon ablation of other materials which evaporate as clusters of *various shapes*. Among these are polymers (see, for example, [9–13]), higher carbon oxides [14, 15], and soot produced upon benzene combustion [16]. Fullerene C_{60} can be synthesized in a reactor filled with a mixture of C_2H_2 and He [17], as well as with a mixture of C_2H_2 and SF_6 [18, 19]; fullerenes also arise in a flame [20, 21];

(3) The mass spectra of fullerenes enriched by isotope ^{13}C and studied in Ref. [22] cannot be explained by fullerene assemblage from graphite fragments. The fullerenes in that experiment were produced under conditions optimal for synthesis in an arc discharge between graphite electrodes. In graphite containing 98.9% ^{12}C, holes were made, which were filled with amorphous ^{13}C. If the main channel for the formation of fullerene C_{60} is the assembly of graphite sheets consisting of tens of atoms, the mass spectrum should reveal fullerenes formed from the graphite carbon alone and, hence, consisting mainly of ^{12}C. However, the mass spectrum observed in the experiment indicated that the carbon atoms mixed completely in the plasma before precursor clusters arose.

2.3 'Nautilus' model

Another model for fullerene formation will be referred to, for brevity, as the 'nautilus' model [23–27]. According to the model, a carbon cluster growing in a plasma during fullerene synthesis looks like a curved sheet, where carbon bonds are arranged in pentagons and hexagons, as in the fullerene structure. While growing the sheet rolls up itself so as to minimize the number of free bonds. The growth of the carbon cluster is similar to that of a snail shell (Fig. 2). Some growing clusters can accidentally close into fullerenes. Others grow further forming 'quasi-spiral' soot particles. The model does

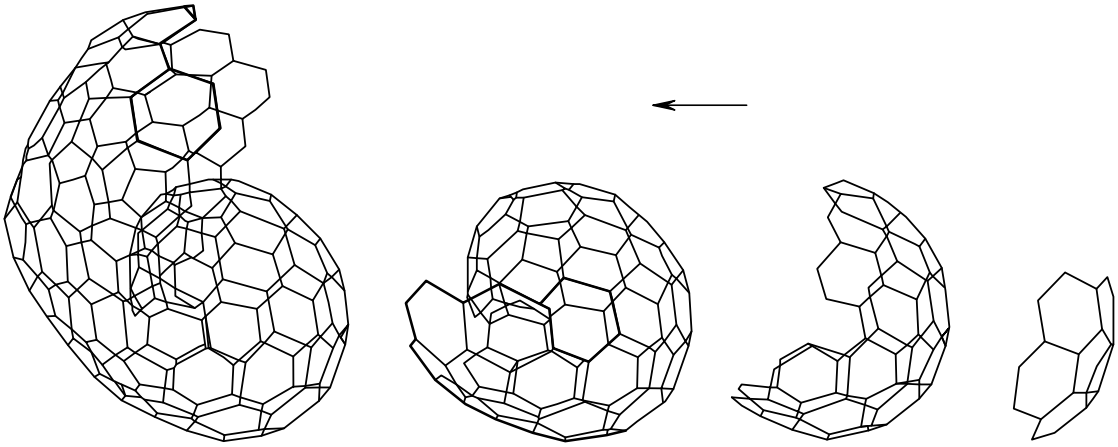

Figure 2. The growth of a carbon cluster according to the 'nautilus' model [25].

not relate fullerene formation only to graphite evaporation, but it cannot explain the high yield of fullerene C_{60} under certain conditions of synthesis (see, for example, [8, 28]). Moreover, studies of the second ionization potential and thermal ion emission of great carbon clusters up to C_{300}, assembling together with C_{60}, reveal them to be fullerenes rather than quasi-spiral particles [29]. It was proposed in [8] that soot in flames also forms according to the nautilus model. However, there is evidence contradictory to the hypothesis that soot particles formed in flames exhibit a 'quasi-spiral' shape: (1) soot particles contain atoms of O, H, and other elements [30, 31]; (2) chemical properties of soot particles are closer to those of benzene than to those of graphite [30, 31]; (3) NMR studies of soot particles show that they include polycyclic aromatic hydrocarbons [30, 31]; (4) the X-ray scattering spectrum of soot is more similar to those of polycyclic aromatic hydrocarbons than to that of graphite [31].

2.4 Assemblage from clusters

In this section we analyze the models, according to which fullerenes assemble from various clusters whose structure coincides with that of 'fullerene fragments'. The drawbacks of the above models are corrected by the 'pentagon rule' [32, 33]. According to this model, a growing carbon sheet anneals so that the pentagons are maximally separated by hexagons, eventually producing fullerene C_{60}. The overwhelming majority of carbon clusters larger than C_{30} contains only even numbers of atoms (see, for example, [1, 12, 34]), therefore the pentagon rule was improved by the assumption that the growth of C_{60} occurs through the successive addition of C_2 [35]. Some schemes of C_{60} and C_{70} formation from C_2 according to the improved pentagon rule are given in [36]. There are several models for the assemblage of fullerenes from larger precursors, namely: C_{60} from three C_{20} [36]; C_{60} from six C_{10} [2, 3, 37]; the 'ring stacking' model (Fig. 3) where $C_{10} + C_{12} + 2C_{18} + C_2 = C_{60}$ [38, 39], $2C_{10} + 2C_{20} + C_{24} = C_{84}$ [40], $C_{10} + C_8 + C_{20} + C_{16} + 3C_2 = C_{70}$ [39], and a number of ways of assembling from other similar precursors [41].

The authors of the 'ring stacking' model [38–40] believed that their model could be verified by the NMR detection of isomer C_{84} with a certain symmetry [42]. But a more recent NMR study [43] did not reveal this isomer.

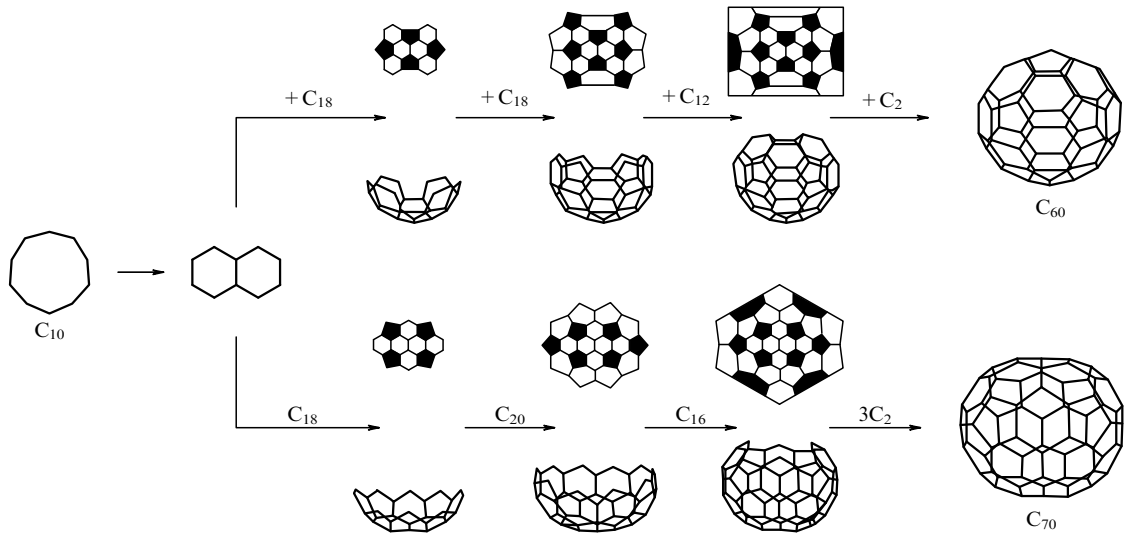

Figure 3. The assemblage of fullerene C_{60} according to the 'ring stacking' model [38].

The above models of fullerene formation [32, 33, 35–41] imply the existence of certain cluster-precursors C_n whose structure is similar to that of 'fullerene fragments'. Such precursors are assumed to be polycyclic plane sheets at $n = 10-19$, and curled polycyclic cup-like sheets involving only pentagons and hexagons at $n > 20$. On adding hydrogen to a buffer gas during fullerene synthesis (to interrupt it), polycyclic aromatic hydrocarbons C_nH_m with $n = 15-20$ were obtained [36], whose structure was similar to that of the carbon clusters acting as fullerene precursors in some models [32, 33, 35–41]. But this fact does not prove that the hot carbon clusters which formed the hydrocarbons on cooling of the plasma had the same sizes and structure. On the contrary, both theoretical calculations of the energy of various carbon clusters [44–47], and experimental study of cluster mobility [48–51] and the electron photoemission spectrum [52] show that such clusters, consisting of 15–20 atoms, are monocyclic rings. Moreover, precise *ab initio* calculations of the carbon cluster structures (using molecular dynamics approach combined with the density functional method [46], and the quantum Monte Carlo technique [47]) indicate that the bicyclic cluster C_{10} is not stable even at zero temperature, although the models [37–41] require its possible existence. Any polycyclic clusters consisting of 11–13 atoms are also unstable [47]. The structure of the first stable polycyclic cluster C_{14} is three-dimensional and not planar as the 'ring stacking' model requires (Fig. 4) [47]. Other data on clusters derived from graphite ablation studies do not confirm the assumption that carbon clusters C_n with $n = 10-20$ make polar polycyclic sheets consisting of pentagons and hexagons. The analysis of the mass spectrum of hydrocarbons produced as a result of laser ablation of graphite in the presence of hydrogen indicated that the initial carbon clusters C_n with $n = 10-20$, which accepted hydrogen, were chains and rings. But these data do not exclude the existence of bicyclic clusters [53]. A similar experiment with carbon plasma revealed chains containing up to 44 atoms [54]. The photoemission spectrum of carbon clusters demonstrated the rings up to $n = 29$ [52]. Calculations on carbon cluster isomers show that the binding energy of rings at $n < 25$ and fullerenes at $n > 20$ exceeds that of the cup-like clusters consisting of pentagons and hexagons [44]. Studies of the mobility of carbon clusters demonstrate that clusters C_n are chains for $n < 10$, rings for $7 < n < 40$, bicyclic clusters for $21 < n < 40$, and that tricyclic and polycyclic clusters and fullerenes appear at $n > 30$ [49, 50]. It is significant that, according to molecular dynamics simulations, hot clusters at $n \geqslant 30$ already have a three-dimensional structure with a closed surface even at 3000 K [55]. In view of these facts it seems unlikely that cluster cups formed of pentagons and hexagons alone can be precursors of fullerenes during their synthesis. Even more doubtful is the existence of such clusters of a certain form which are the fragments of the most abundant fullerene C_{60}.

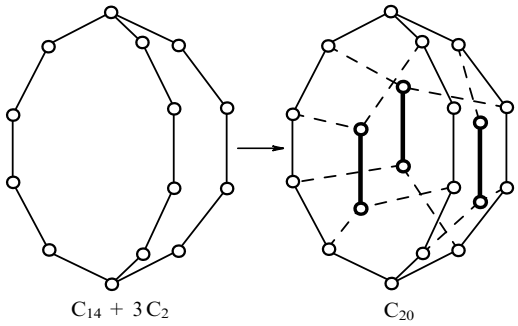

Figure 4. The structure of cluster C_{14} in the ground state [47] and the scheme of its growth into C_{20} fullerene by insertion of C_2 microclusters to its structure [59]. The bonds formed during the insertion process are shown by dashed lines; the bonds between the atoms of added C_2 microclusters are distinguished by bold lines.

At the same time we cannot fully deny the existence of nonequilibrium clusters having the structure of fullerene fragments. The concentration of such clusters in plasma can decrease rapidly after their formation if the clusters react intensively with each other (for instance, with the production of fullerenes and other nanostructures). In this case the experimental detection of such clusters would be very difficult.

Notice that models of fullerene assemblage similar to 'ring stacking' may adequately describe fullerene formation as a result of chemical reactions between polycyclic hydrocarbons, such as the synthesis of fullerene C_{60} in a flame [56] and during naphthalene pyrolysis [57].

2.5 'Fullerene road'

A model referred to as the 'fullerene road' was suggested in [58]. According to the model, a fullerene arises from a carbon cluster consisting of 30–40 atoms, further clustering occurring by the insertion of C_2 microclusters (see Fig. 5). However, as we will discuss at length in what follows, experiments demonstrate that the cluster transformation into fullerenes is possible also for clusters containing a hundred atoms and more (see, for example, [16]). Nevertheless, the idea of the possible growth of fullerenes after their formation can be useful to explain the large yield of some fullerenes (for instance, C_{60}). We will consider this question in Section 3.

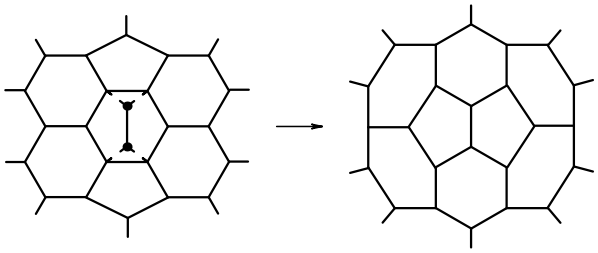

Figure 5. The scheme of insertion of a C_2 microcluster into a fullerene [97].

Small fullerenes were proposed to form by the repeated insertion of C_2 clusters into three-dimensional polycyclic carbon clusters [59]. According to some calculations, the binding energy of a fullerene is the highest among isomers of a C_{20} cluster (see Refs [44, 60, 61]). Figure 4 plots a scheme of fullerene formation from a C_{14} cluster by insertion of C_2. The plotted structure of the C_{14} cluster corresponds to its ground state (see calculations using quantum Monte Carlo simulations [47]).

2.6 Annealing of carbon clusters

Fullerene formation was explained in Refs [15, 49, 50, 59, 62–66] through the annealing of carbon clusters. The possibility of this mechanism is confirmed by the following experiments.

(1) Studies on the mobility of carbon clusters in a chromatographic cell demonstrate that bi- and tricyclic

clusters consisting of 34 – 60 atoms anneal into fullerenes with the emission of atoms or microclusters [62, 63].

(2) Laser ablation of higher carbon oxides produces the rings C_{18}, C_{24}, and C_{30}, which stick together into large clusters, and then anneal into fullerenes with the emission of 2 – 10 atoms [15].

(3) Fullerenes containing hundreds of atoms are annealed from clusters arising from sticking together the C_{60} fullerenes during the ablation of pure C_{60} film [67].

(4) Metallofullerenes with two and three metal atoms inside the fullerene shell are produced only by two- and three-fold laser ablation of a certain sample area [68, 69]. It was assumed [68] that metallofullerenes with two internal metal atoms were formed from clusters appeared as a result of sticking together two metallofullerenes with a single internal metal atom, while the metallofullerenes with three metal atoms by sticking together metallofullerenes with one and two internal metal atoms [68].

The following scheme was suggested in Ref. [49] for the growth and annealing of a carbon cluster in a plasma: chain – ring – three-dimensional polycyclic cluster – transformation into fullerene. For example, three-dimensional polycyclic clusters growing and annealing with transformation into fullerenes can be formed in the following ways: the sticking of a chain and a ring, the sticking of rings, and the transformation of bicyclic and tricyclic clusters into polycyclic clusters [59]. Figure 6 plots the proposed means of polycyclic cluster formation as well as the scheme of fullerene formation. Originally, a plane structure was suggested for bicyclic [51] and tricyclic [50] clusters (see Fig. 6a), the calculated mobility of the clusters corresponding to experiment. However, later [70] a three-dimensional structure for such clusters was proposed (see Fig.7) which also provided results consistent with experiment. Moreover, a similar three-dimensional structure of such clusters was found by quantum-chemical calculations for two joining rings [71]. The structure of tricyclic carbon clusters was also suggested to be

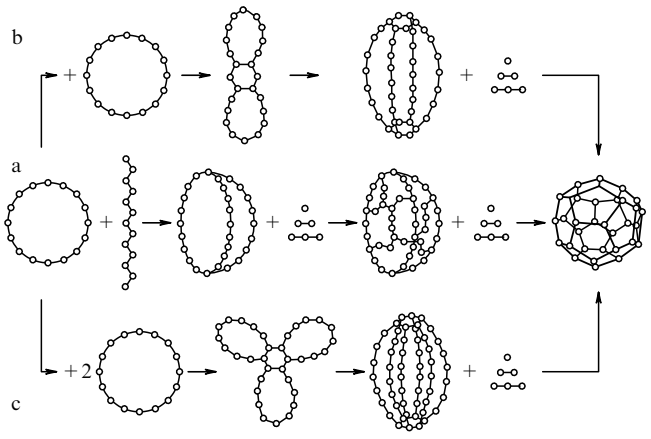

Figure 6. The scheme of growth of a carbon cluster accounting for the following stages: chain — ring — three-dimensional polycyclic cluster — transformation to the fullerene. Different ways for the formation of a three-dimensional polycyclic cluster are shown: (a) a chain and monocyclic ring form a three-dimensional tricyclic cluster transforming into the three-dimensional polycyclic cluster; (b) two monocyclic rings form a plane bicyclic cluster transforming into the three-dimensional polycyclic cluster; (c) three monocyclic rings form a plane tricyclic cluster transforming into the three-dimensional polycyclic cluster [59].

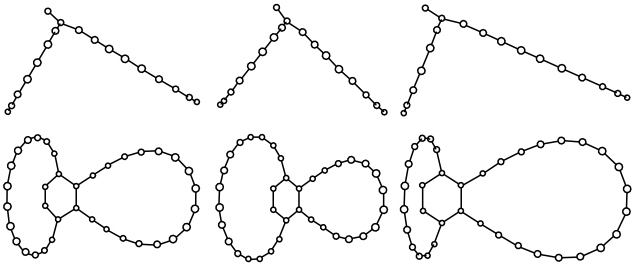

Figure 7. The structure of three tricyclic clusters C_{36} [70] illustrated via their projections on the mutually orthogonal axes.

similar to that of a C_{14} cluster in its ground state, as calculated by the quantum Monte Carlo method [47] (see Fig. 4).

Let us consider now possible ways for the formation of the carbon clusters which anneal into fullerenes. In contrast to various models of 'fullerene assemblage', these ways do not imply a specified structure for fullerene-precursor clusters. During graphite ablation, carbon clusters arise from sticking together the atoms and microclusters consisting of several atoms, which is closely confirmed by kinetic calculations [13, 72]. Notice that clustering from carbon vapor can occur either as a homogeneous nucleation (formation of liquid nuclei in a metastable supersaturated vapor) or as a spinodal decomposition into thermodynamically unstable phases. This question is detailed in [64, 66, 73]. Another possibility for the formation of great carbon clusters is the sticking of several clusters containing tens of atoms. This process takes place during the ablation of higher carbon oxides [15]. The mass spectrum of carbon clusters produced by soot ablation indicates that both ways are possible [16]. This mass spectrum exhibits two maxima in the fullerene distribution. The first maximum ($n = 154$) corresponds to the sticking of atoms and microclusters, while the second ($n = 450 – 500$) is caused by the sticking of clusters containing tens of atoms. Fullerenes also arise from the initially large clusters evaporated from the carbon-containing material, for example, during the evaporation of a finely divided graphite foil [28] or during the secondary laser ablation of a certain area of graphite surface [68].

Two ways were proposed for the annealing of a carbon cluster into a fullerene. According to the first, a polycyclic cluster transforms gradually through sequential transitions from one isomer into another [71, 74]. The second implies the crystallization of a liquid cluster [59 – 66]. The gradual cluster transformation into a fullerene was calculated for a plane tricyclic cluster C_{60} [74] (see Fig. 8) and for a three-dimensional tricyclic cluster C_{36} [71] (Figs 9 and 10). The plane cluster transforms into the highly prolate fullerene C_{60} with numerous defects like heptagons and osculating pentagons. Moreover, the calculated time of this transformation ($\geqslant 10^{-3}$ s [71]) depends strongly on the initial structure of the tricyclic cluster, and even for such an 'irregular fullerene' it exceeds the experimentally established time of fullerene formation, which is about 10^{-9} s [10]. For the three-dimensional tricyclic cluster C_{36}, its transformation into fullerene does not result in the isomer with the highest binding energy, however the energy released during the process is enough to overcome the activation barrier of the transition reaction distinguishing the fullerene isomers.

The model for the transformation of a polycyclic cluster into a fullerene does not take into account the emission of

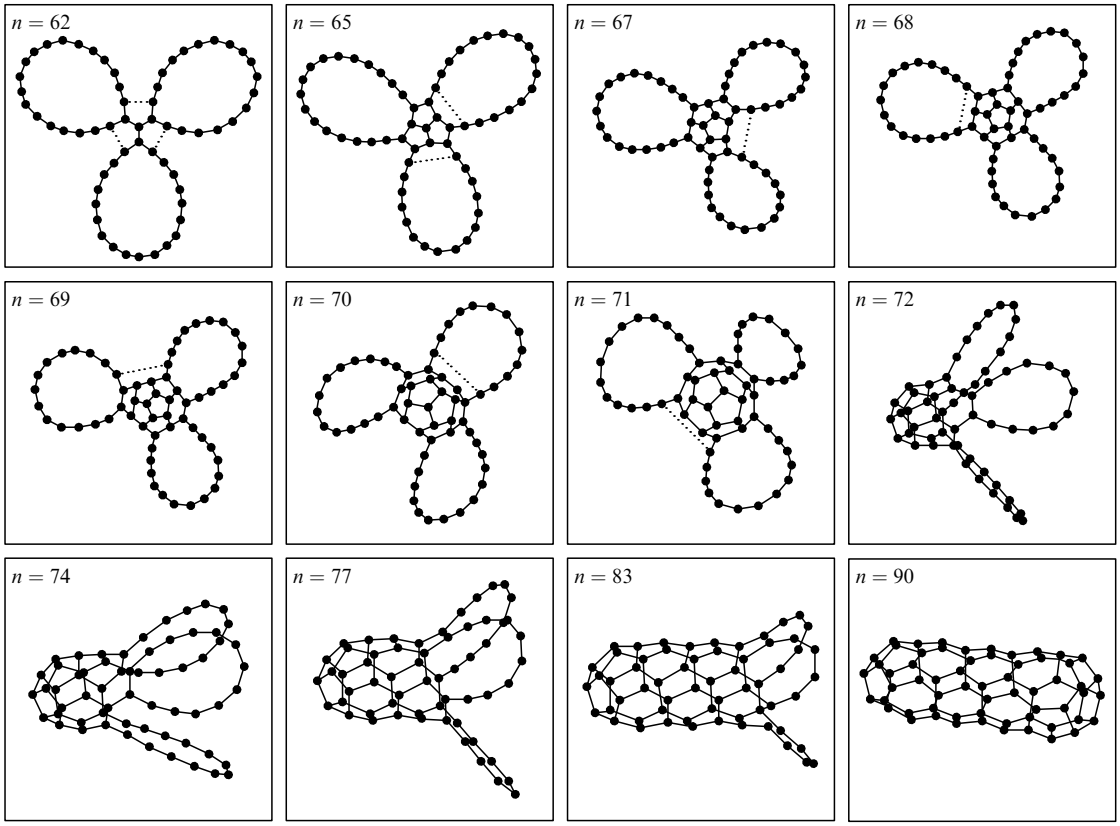

Figure 8. The transformation of the plane tricyclic cluster C_{60} into a fullerene [74]; n is the number of cluster bonds.

atoms and microclusters during the process. However, as pointed out above, the emission of atoms and microclusters during carbon cluster annealing to the fullerene was revealed in a number of experiments (see, for instance, Refs [15, 62, 63, 67]). Emission of atoms and microclusters is possible for a liquid cluster. Following the above arguments, we believe that the crystallization of a liquid cluster is a more probable way for the cluster transformation into a fullerene than the gradual transformation of a polycyclic cluster. Nevertheless, we think that depending on the initial temperature of the cluster and the annealing time, the cross over is a possibility and one behaviour can merge into the other.

Thus, we believe fullerene formation to occur as follows: first, liquid carbon clusters are formed, then these clusters crystallize into fullerenes with the emission of atoms and microclusters. This scenario can be used to explain some experimental facts:

1. NMR study of C_{60} fullerenes enriched with the isotope ^{13}C reveals that neighbouring ^{13}C atoms in an amorphous graphite are not neighbours in fullerenes [75, 76]. This means that either C_2, C_3, and other microclusters are absent from the products of amorphous graphite evaporation or, in accordance with the considered model of crystallization, atoms mix in a liquid cluster before its crystallization into a fullerene.

2. Some experiments on carbon clusters containing 30 – 40 atoms show that there is a 'dead region' in the mass spectrum, corresponding to small amounts of clusters (see, for example, [77]). It has been proposed that the clusters from this region decayed by emitting clusters containing more than 10 atoms [72]. We offered an alternative explanation of the 'dead region' [59]. In fullerenes containing 30 – 40 atoms the binding energy per atom is less than in larger fullerenes [44]. Therefore, carbon clusters with 30 – 40 atoms have a lower temperature of crystallization and crystallize at a later time into fullerenes on plasma cooling, hence, they have enough time for growing into larger clusters, with a consequent essential reduction in the amount of clusters related to the mass-spectrum 'dead region'. This explanation is confirmed by the calculations of the kinetics of carbon cluster growth [78]. We do not exclude the possibility that the 'dead region' arises as a result of fullerene growth after formation (see the next section).

3. Special ways for the assemblage of metallofullerenes with an internal metal atom were proposed (see, for example, [79]). We suggest here a simple scenario: a metal atom appears inside a fullerene during the crystallization of a liquid cluster.

Rare gas atoms were found inside fullerenes after their formation [80]. The 'window opening' mechanism was proposed to explain this experiment [81]: C – C bonds in a fullerene rearrange for a short time to form a higher sized ring instead of a six-membered ring, through which the atom enters the fullerene.

2.7 Crystallization of a liquid cluster into a fullerene

In this section we discuss the process of crystallization of a liquid cluster into a fullerene. Different nuclei for fullerene crystallization were proposed: a cluster with a Cayley tree structure (Fig. 11) [64, 66, 82], and a C_{20} cluster with a corannulene molecular structure, i.e. a curled sheet comprising a pentagon surrounded by hexagons (Fig. 12) [55]. We advance here some arguments in favour of the second hypothesis. Firstly, according to calculations [83], a cluster

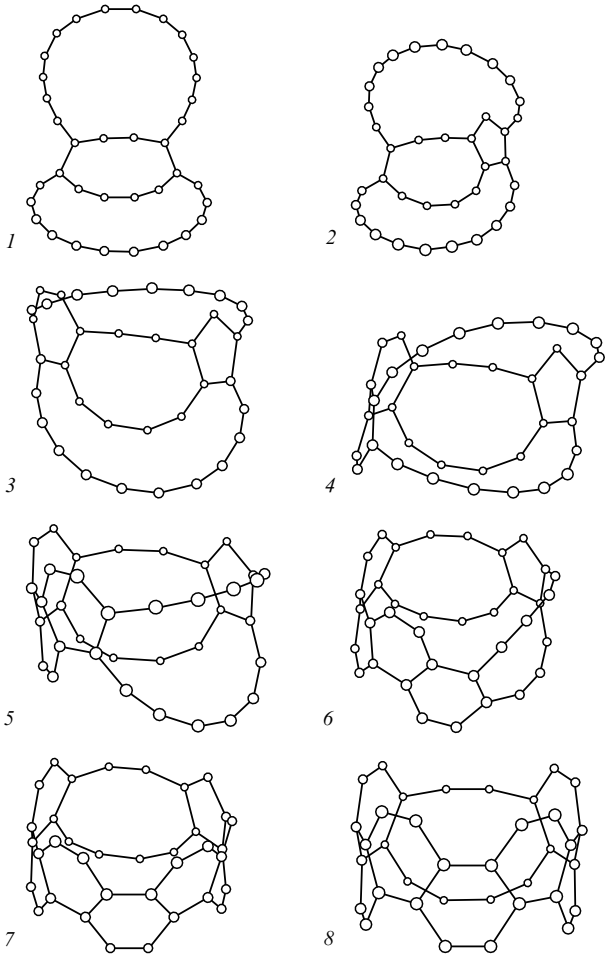

Figure 9. The transformation of the 3D tricyclic cluster C_{36} into a cylindrical cluster [71].

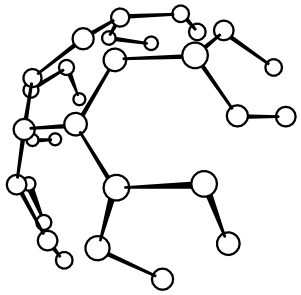

Figure 11. The 30-atomic tree carbon cluster embedded in the spherical surface of a liquid cluster [64].

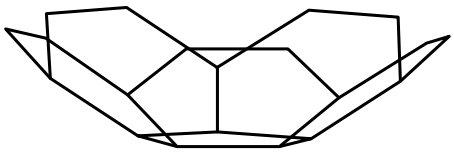

Figure 12. Cluster C_{20} with the structure of a corannulene molecule [83].

with a corannulene molecular structure has the highest binding energy among the isomers of C_{20} and is stable up to 4500 K. Secondly, to form the spheroidal fullerene structure, energy is spent to curl the graphite sheet. A cluster with the structure of a corannulene molecule in the ground state is already curled unlike graphite sheet which does not contain a pentagon. Therefore, if a cluster is a nucleus for fullerene crystallization, less energy is spent to curl the growing sheet. The rest of the fullerene crystallizes around one or several nuclei, as in the crystal growth in liquids.

All fullerenes have an even number of atoms, since the polyhedra always have even number of vertices. In most cases the mass spectrum of carbon clusters produced by the ablation of carbon-containing materials include scarcely any clusters with an odd number of atoms (see, for example, [12, 16]). The absence of such clusters can be explained by the emission of atoms and microclusters during crystallization, which agrees with some experiments and calculations. For

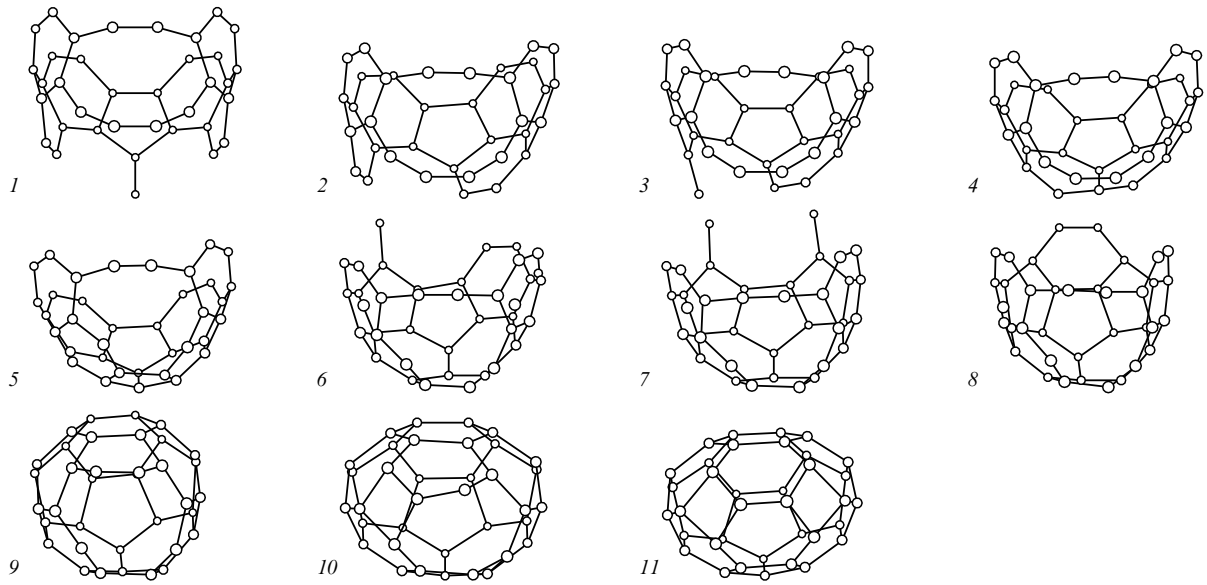

Figure 10. The transformation of the cylindrical cluster C_{36} into a fullerene [71].

example, experiments on the mobility of carbon clusters revealed that a cluster with an odd number of atoms transforms into a fullerene after the emission of an 'excess' atom [62, 63]. The mass spectrum of carbon clusters produced by graphite ablation in a vacuum [12] coincides with the spectrum found by chemical kinetics calculations accounting for odd clusters emitting an 'excess' atom.

Clusters with an odd number of atoms always have structural defects. However, such clusters arise in abundance simultaneously with fullerenes on fast cooling of a carbon plasma, and hence on fast annealing of liquid clusters. For example, clusters with an odd number of atoms were produced by laser ablation of graphite into a jet of cold dense buffer gas and their number amounted to about half the fullerenes [28]. We believe that most fullerenes produced under the same conditions have structural defects. This possibility agrees with molecular dynamics simulations, where such fullerenes were found on fast annealing of a liquid carbon cluster over 20 ps [84], 30 ps [85], and 100 ps [86]. We infer that the arising structural defects are typical to the crystallization of a liquid cluster into a fullerene. We also think that the final fullerene structure arises due to transitions from one fullerene isomer to another accompanied by microcluster emission and absorption. We shall consider this problem in the next section.

3. Magic fullerenes and fullerene isomers

3.1 Set of magic fullerenes

In this review the term 'magic fullerenes' is used to mean fullerenes produced in abundance relative to other fullerenes under certain conditions. In addition to C_{60}, another fullerene produced in high yields is the fullerene C_{70}. Some other fullerenes are magic under certain conditions of synthesis: (1) C_{28} during laser ablation of graphite in a buffer gas heated to 1200 K [87], (2) C_{78} and C_{84} when extracted from soot produced in the arc discharge between graphite electrodes [8]; (3) C_{32} and C_{50} obtained in a Fourier mass spectrometer using a magnetic field to retard the expansion of plasma containing the fullerene mixture [87]; (4) C_{36} [88], C_{44} [9], C_{50} [9, 88], and C_{76} [88] on fast cooling in a supersonic jet of cold buffer gas; (5) C_{44} and C_{50} in the upper part of a flame [20]; (6) C_{76} among the photodecomposed products of fullerenes C_{94} [89], and C_{36} [90], C_{44}, C_{50} [90, 91] among the products of C_{60} photodecomposition; (7) C_{36}, C_{44}, and C_{50} in a chemical reactor filled with a mixture of C_2H_2 and SF_6 [18]. Sometimes the mass spectrum exhibits no magic fullerenes. This is the case, for example, with fullerenes produced during ablation of carbon-containing materials in a vacuum [9, 11, 12] or in a supersonic jet [28, 34, 88].

3.2 Role of fullerene transformations

In the pioneering paper [1] devoted to fullerenes the high yield of fullerene C_{60} was observed only when the carbon plasma had been held in a small vessel before expansion. The high yield of C_{60} was inferred to result from cluster-cluster reactions before the plasma expansion. These reactions were more recently proposed to be the emission and insertion of microclusters by fullerenes as well as fullerene exchanges of the microcluster C_2 [92]. We discuss below the linkage between the high yield of magic fullerenes under various conditions and the magnitudes of rate constants of the insertion $C_n + C_2 = C_{n+2}$ and emission $C_n = C_{n-2} + C_2$ reactions.

Numerous experiments indicate transformations of fullerenes between each other. It was found that in most cases fullerenes decay with the emission of the microcluster C_2 to form smaller fullerenes [77, 90]. This phenomenon is attributable to the fact that fullerenes always have an even number of atoms. The binding energy of the microcluster C_3 per atom exceeds that for the microcluster C_2 (see, for example, [45]), therefore other carbon clusters decay with the emission of C_3 [77, 90]. According to experiments on the IR-spectrum of carbon plasma produced by laser graphite ablation, C_3 microclusters were detected in the plasma region near the target, while the C_2 microclusters were found far from the target [93]. At equilibrium in the carbon plasma the concentration of C_3 microclusters exceeds the concentration of C_2 microclusters by a factor of several tens [94]. Therefore, C_2 microclusters found far from the target were interpreted in [93] to result from the transformation of larger fullerenes into smaller ones with the emission of a C_2 microcluster.

The insertion of C_2 into fullerenes was revealed in the study of laser ablation of fullerite [95]. If the laser pulse is weak, the mass spectrum of evaporated fullerenes contains only the C_{60}, C_{70}, and C_{84} that make up fullerite. As the pulse energy increases, other fullerenes arise, namely, C_{50}, C_{56}, C_{58}, and all the fullerenes containing from 72 to 110 atoms. The fullerenes C_{50}, C_{56}, and C_{58} probably appeared as a result of the decay of C_{60}. The fullerene C_{62} is not observed in the mass spectrum involved. This means that C_{60} does not take up C_2 under these conditions. The insertion of microclusters larger than C_2 into the C_{60} fullerene is even less probable, since this reaction proceeds with breaking of greater number of bonds than the reaction of C_2 insertion and, hence, an increased activation barrier must be overcome. Therefore, the fullerene C_{72} could be produced in experiments only by the insertion of a C_2 microcluster into fullerene C_{70}. The fullerenes $C_{74}-C_{110}$ arise due to repeated insertion of microcluster C_2 and, probably, other microclusters into fullerenes C_{70} and C_{84}. The laser desorption of fullerenes separated by chromatographic technique not only demonstrates the possibility of C_2 insertion into fullerenes but also indicates indirectly different rates of this reaction for various fullerenes. For instance, under the same desorption conditions fullerenes C_{78} and C_{84} do not take up the C_2 microcluster, while fullerenes C_{76} and C_{82} adsorb it, whereas C_{90} and C_{96} adsorb even two C_2 [39, 96]. The possibility of fullerene transformations between each other is confirmed by the experimental fact that the concentration of C_{60} increases in the upper part of a flame with decreasing concentration of other fullerenes [21]. A scheme of insertion of the microcluster C_2 into fullerenes was proposed in Ref. [97] (Fig. 5). The calculations [92] indirectly confirm that the reaction rate for the insertion of C_2 into C_{60} decreases with respect to that for C_{58}. These calculations also reveal that a certain orientation of the microcluster C_2 is required for the insertion into C_{60} as distinguished from the C_{58} case. Another reaction of C_2 insertion, i.e. $C_n + C_3 = C_{n+2} + C$ was also proposed in Ref. [98].

The fullerenes C_{36}, C_{44}, and C_{76} are magic among fullerenes produced by photodecomposition of large fullerenes [89, 90]. Therefore, we believe that the rate constant k^- for the reaction $C_n = C_{n-2} + C_2$ of C_2 microcluster emission is low for these fullerenes. Thus, the significant peaks in the mass spectrum corresponding to fullerenes C_{36}, C_{44}, and C_{76} indicate the important role of this reaction in the selection of magic fullerenes under these conditions. Particularly, such peaks are observed on ablation of carbon-contain-

ing materials in a jet of cold buffer gas [9, 88]. Some fullerenes are magic when an expansion of carbon plasma is retarded by a magnetic field in a Fourier-transform mass spectrometer (for instance, fullerene C_{32} [87]) or by a hot inert buffer gas (fullerenes C_{28} [87], C_{84} [68]). We think that under the conditions of longer plasma confinement the reaction of insertion into fullerenes is important. Therefore for fullerenes C_{28}, C_{32}, and C_{84} the rate constant k^+ of the reaction $C_n + C_2 = C_{n+2}$ is low. Fullerenes C_{50}, C_{60}, and C_{70} are magic under various conditions of synthesis. We suppose that for these fullerenes both constants k^+ and k^- are lower than for other fullerenes.

The measurement of the decay constants for several fullerenes demonstrate that these constants are actually lower for magic fullerenes C_{60} [99, 100] and C_{70} [99] than for other fullerenes of 'neighbouring' sizes. However, the difference in the decay constants can explain the observed ratio between the numbers of fullerenes, which varies greatly [1] and under optimal conditions amounts to tens. The number N_n of fullerenes consisting of n atoms decreases exponentially as a result of their decaying:

$$N_n = N_{n0} \exp(-k_n^- t) ,$$

where N_{n0} is the initial number of fullerenes, k_n^- is the rate constant of emission of C_2 microclusters by these fullerenes (as mentioned above, it is the main channel of fullerene decay). Hence, the ratio N_n/N_m between the numbers of fullerenes consisting of n and m atoms also decreases exponentially in time:

$$\frac{N_n}{N_m} = \frac{N_{n0}}{N_{m0}} \exp\left[-(k_n^- - k_m^-)\, t\right] .$$

Moreover, these measurements were carried out for hot as-formed fullerenes arising under conditions not optimal for producing magic fullerenes. Since $k^- \approx \exp(E_a/kT)$, where E_a is the activation energy, the ratio of these constants rises as the temperature decreases. Thus, the fullerene mixture can be enriched with magic fullerenes by the exposure of carbon plasma containing fullerenes at the optimal temperature.

Nevertheless, under certain conditions fullerene C_{70} is the most abundant, for example, during graphite ablation by electrons or helium ions [101], and in producing fullerenes in arc discharge when graphite electrodes contain hafnium carbide [102]. When fullerenes are produced in an arc discharge the fraction of C_{70} and other higher fullerenes increases several times if the electrodes are doped with boron, aluminium or silicon, while the buffer gas contains nitrogen [103]. The reason for these effects is not clear. We believe that in the above cases clusters containing about 70 atoms are more abundant by the time of onset of the liquid clusters crystallization into fullerenes than clusters containing about 60 atoms. We also do not rule out the possibility that the rate constants k^+ and k^- are lower for fullerene C_{70} than for fullerene C_{60} under certain conditions. Fullerene C_{70} is more abundant in flames [20], probably for another reason. As we noted above, the model of fullerene assemblage from hydrocarbons may be correct for this flame experiment [56]. Then the abundance of fullerenes is determined by the assemblage processes.

The set of 'empty' magic fullerenes (C_{60}, C_{70}, C_{76}, etc.) does not coincide with the set of magic metallofullerenes. For example, fullerene C_{82} is magic only with an internal metal atom (see [104] and references therein). Some special ways for assembling this metallofullerene were proposed [79]. We suggest here a simple explanation, namely, the rate constants k^+ and k^- for metallofullerenes differ from those for 'empty' fullerenes containing the same number of atoms.

3.3 Energetics and structure of magic fullerenes

It was assumed that the greater the number of osculating pentagons on a certain area of the fullerene surface, the lower the binding energy per atom from this area, and hence, fullerenes were magic when they had peculiarities in the distribution of pentagons [105]. Actually, the structure of some magic fullerenes do have such peculiarities [105], for example, fullerenes C_{28} and C_{32} are the smallest fullerenes in which the groups of three osculating pentagons are pulled apart, C_{50} is the smallest fullerene in which the pairs of osculating pentagons are pulled apart, C_{60} and C_{70} are the smallest fullerenes in which all the pentagons are separated. We suppose fullerene surface areas with osculating pentagons to have not only a lower binding energy per atom but also a lower activation energy of C_2 microcluster emission. Therefore these surface areas emit a C_2 microcluster easier. Thus, fullerenes where pentagons are maximally separated by hexagons, survive as a result of the C_2 emission reactions in the mixture of fullerenes. The possibility of the C_2-fullerene insertion reaction is also determined by the local fullerene structure. As we mentioned above, to insert C_2 into the fullerene C_{60}, the microcluster C_2 should be certainly oriented as opposed to that for fullerene C_{58} [92]. Notice that the assumption about the correlation between the fullerene structure and binding energy is in agreement with calculations, viz. the average binding energy E_n per atom increases with n for $n = 60-96$ [106]. Only the magic fullerenes C_{60}, C_{70} and C_{84} are exceptions to this rule, but for these clusters E_n is greater merely by 5.7, 1.9 and 0.6% than for C_{62}, C_{72}, and C_{86}, respectively.

3.4 Formation of fullerene isomers

The mixture of fullerenes extracted from arc-discharge-produced soot dissolved in toluene or benzene contains many other fullerenes in addition to C_{60} and C_{70}, whose content amounts to 98%. However, only a single isomer of each of C_{60} and C_{70} was detected in the mixture. Several possibilities explaining the selection of certain isomers were proposed.

One of them is isomer transformations between each other. The simplest transformation of this kind is the Stone–Wales reaction consisting in the permutation of two bonds [107], depicted in Fig. 13. According to the calculations, this reaction has a significant activation barrier nearly

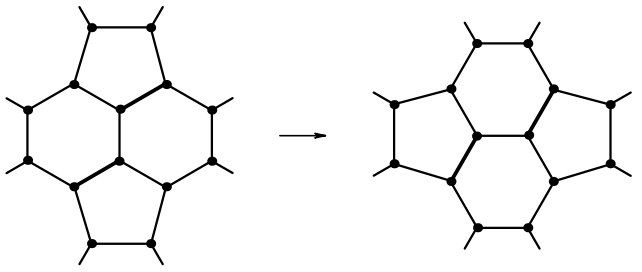

Figure 13. The scheme of the simplest reaction of fullerene isomer transformation by the permutation of two bonds [107].

5 – 8 eV [135, 109]. The energy required to overcome the barrier may be released by C_2 insertion [92] or by the transformation of a polycyclic cluster into a fullerene [71]. The activation barrier of the Stone – Wales reaction can decrease to 3 eV due to autocatalysis by a carbon atom [109]. The autocatalysis by C_2 and C_3 microclusters (whose concentration in carbon plasma exceeds the concentration of carbon atoms [94]) further decreases the activation barrier for this reaction [110]. But in this case a carbon atom or microcluster must be chemisorbed from carbon plasma just onto the fullerene surface area, where the bond between the fullerene atoms breaks according to the Stone – Wales reaction. Moreover, we believe a mixture of isomers to result from above isomer transformations. For example, such an isomer mixture arises at a temperature of only 1300 K when examining reactions between the isomers of polycyclic hydrocarbons $C_{16}H_{10}$ [111]. In the review [98] some other reactions of isomer transformations between each other are also considered. However, these reactions are accompanied by a large number of broken bonds, and therefore, have an increased activation barrier.

Another assumption about the selection of certain isomers is that the fullerene structure formed during the crystallization of a liquid carbon cluster is restricted by the spherical surface of the cluster [65]. Thus, the formation of nonspherical fullerenes is eliminated. We think that only rather prolate isomers may be excluded by this isomer selection. For example, the very abundant fullerene C_{70} is slightly oblong. Moreover, the authors of [65] reason that carbon nanoparticles with a shell structure also result from liquid cluster crystallization. Nevertheless, the shape of these nanoparticles is more similar to a polyhedron than to a sphere. Therefore, the spherical shape of liquid carbon clusters is not retained during the crystallization. The formation of carbon nanoparticles will be discussed in detail in the next section.

Conceivably, fullerene crystallization might follow the 'pentagon rule' path. (As indicated above, this rule was proposed to explain fullerene growth [32, 33]). For the fullerene C_{60} with icosahedral symmetry such crystallization is only a repetition of the initial nucleus C_{20}. Thus, we suppose that the crystallization of a liquid cluster into a fullerene could be a way for selecting certain isomers.

As for the selection of magic fullerenes, the main mechanism of fullerene isomer selection is probably the reactions of C_2 insertion and emission. As mentioned above, we believe the rate constants of the reactions to be determined by the local structure of the fullerene surface areas emitting or inserting C_2 microcluster. Hence, isomers with a certain structure are selected by these reactions. Notice that the simplest reaction of isomer transformations between each other has a significant activation barrier (about 5 – 8 eV) [135, 109], while the activation barrier for C_2 emission is approximately half (about 3 – 4 eV) [100], whereas C_2 insertion into a fullerene occurs without overcoming a barrier [92].

It was also inferred that the main mechanism of isomer selection is the microcluster exchange reactions at collision of two fullerenes [92], exemplified by

$$C_{58} + C_{62} = 2C_{60} + 5.8 \text{ eV}.$$

Isomers are probably selected by the extraction of fullerenes from soot. Fullerenes smaller than C_{60} are absent among the fullerenes extracted from soot dissolved in toluene, benzene and other solvents (see, for example, Refs [8, 68, 101]). This fact does not imply, however, that such fullerenes are not formed under suitable synthesis conditions. Fullerenes involved cannot be extracted from soot, because they form chemical bonds with neighbouring fullerenes. Such bonds are probably formed by the atoms located at the vertices of two or more pentagons. This suggestion explains the absence of fullerenes less than C_{60} in soot extract, since all of them have osculating pentagons. In the same manner we explain the absence of other isomers of the fullerenes C_{60} and C_{70}, because they also have osculating pentagons. The structure of fullerite from C_{20} and C_{28} was calculated using quantum molecular dynamics approach [112]. Each fullerene in fullerite was found to bond with six neighbouring fullerenes. In the fullerenes C_{20} and C_{28} all the pentagons osculate, so these calculations confirm our assumption.

3.5 Role of the buffer gas

The pressure of the buffer gas must be optimal to produce a maximum yield of fullerene C_{60} at its synthesis in an arc discharge (see, for example, Refs [33, 113, 114]).

According to the model of fullerene assemblage from graphite fragments [3, 4], the role of the buffer gas is as follows. Firstly, it cools the graphite fragments, since being in an excited state they cannot form stable nanostructures. Secondly, it removes the energy released as a result of fragment joining. According to the model, the optimal pressure of the buffer gas derives from the fact that the aggregation of graphite fragments is more difficult under elevated pressures.

We offer two possible explanations of this situation, which are based on the model of liquid cluster crystallization. In the first, we consider the buffer gas effect on the formation of liquid carbon clusters. The size of the arising clusters is determined by the conditions at which nucleation and spinodal decomposition take place, in particular, by the pressure of the buffer gas. To produce fullerene C_{60} at the maximum yield, it is desirable that the size distribution of the liquid carbon clusters before onset of their crystallization should have a maximum near 60 atoms per cluster. Therefore, certain optimal conditions for the liquid cluster growth are necessary, in particular, the pressure of the buffer gas must be optimal.

The second explanation is based on the influence of the buffer gas on the selection of magic fullerenes. The buffer gas can be assumed to retard the expansion of carbon plasma and thus to hold the conditions at which the C_2 microcluster insertion and emission reactions occur. However high pressure of the buffer gas leads to fast cooling of the fullerenes, thus decreasing the reaction rates. Therefore, the optimal pressure of the buffer gas is necessary to select magic fullerenes. In some experiments the dependence of the C_{60} fullerene yield on the buffer gas pressure was found to reveal two maxima (see, for example, [113]), each corresponding to one of the considered buffer gas effects.

The role of the type of buffer gas is not clear. Helium provides the highest yield of fullerene C_{60} under normal conditions in an arc discharge (see, for example, Refs [33, 113, 114]). When argon was used as the buffer gas, the maximal yield of fullerene C_{60} was twice [114], three times [33] or by an order of magnitude [113] less than in the case of helium. The advantage of helium was assumed to be due to the fast relaxation of vibrational excitations in molecules, which are typical of this substance [3, 4]. However, argon provides the highest yield of fullerene C_{60} during laser

ablation of graphite and only small amounts of fullerenes were produced with the use of helium [115].

4. Mechanisms of carbon nanoparticle formation

In this review we consider only the formation of carbon nanoparticles with the structure of graphite layers. The formation of soot particles with different structures is detailed in Ref. [31]. Nanoparticles with graphite layered structures arise in an arc-discharge interelectrode clearance, as with fullerenes [116–118]. Such nanoparticles were also produced from amorphous nanoparticles annealed by an electron beam [119, 120] or in an oven [122], from diamond nanoparticles annealed by an electron beam [122], and during the catalytic pyrolysis of hydrocarbons [123]. Mechanisms for the formation of carbon nanoparticles and fullerenes may be similar, since nanoparticles and fullerenes arise in an arc discharge under rather similar conditions. Therefore, an explanation of nanoparticle formation mechanism could be helpful to understand the mechanism of fullerene formation. Moreover, this explanation could be in use when developing methods for production of new cluster materials.

4.1 Shell structure of nanoparticles and the 'nautilus' model

Images of nanoparticles were first obtained in 1980 [124]. The author reasoned that the structure of these nanoparticles may be considered in the form of closed graphite shells embedded to each other. Transmission electron microscopy with higher resolution (see, for example, Refs [116, 117]) confirmed that conclusion. The chemical bonds between atoms inside the nanoparticle shell are almost analogous to those between the atoms inside a graphite, while the interaction between the atoms of neighbouring shells is described by a weaker van der Waals potential. The shape of the nanoparticle shell usually resembles a polygon (see, for example, Refs [117, 118]). As distinct from the graphite structure each nanoparticle shell involves twelve pentagons in addition to hexagons. Spherical shell nanoparticles can have an additional pentagon-heptagon pairs in their structure [125].

Nanoparticles were initially proposed to have a quasi-spiral structure and to form according to the 'nautilus' model [24, 25]. Nevertheless, as already pointed out in Section 2, this scenario runs into problems at the initial stage of carbon cluster growth in a plasma. Moreover, in most experiments nanoparticles with a large central cavity (see, for example, Refs [117, 118]) were produced. The cavity size is an argument against the main assumption of the 'nautilus' model that the growing carbon sheet curls up in order to reduce the number of 'dangling' bonds.

4.2 Simulation of shell-by-shell growth

Two possible mechanisms for the formation of nanoparticles with a shell structure have been suggested. The first possibility consists in attaching carbon atoms and microclusters to the external nanoparticle shell, producing the subsequent shell (the model of shell-by-shell growth) [25, 117] which, in this case, is formed on the fullerene surface. The second possibility is the crystallization of a liquid cluster [126] or the annealing of an amorphous 'viscid' cluster [118].

A molecular dynamics simulation was used [62, 84–86] to model fullerene formation. However, the very complicated many-particle potential of the atomic carbon interaction and the large number of atoms in the system enabled analysis of the evolution of the system only for 100 ps. This time is not enough for complete fullerene formation, so only fullerenes with numerous defects were simulated.

We used the molecular dynamics approach to simulate shell-by-shell growth of a nanoparticle [127, 128]. Our aim was to calculate the temperature T_{des} at which adsorbed carbon atoms and microclusters are still held on the nanoparticle surface. At an elevated temperature $T > T_{\mathrm{des}}$ atoms and microclusters cannot adsorb onto the nanoparticle surface, so the formation of successive shells is terminated.

In our calculations we used fullerene C_{60} as the first inner shell of a nanoparticle, since the images obtained in Ref. [129] confirm this possibility. We studied a system consisting of fullerene C_{60} and a carbon atom or microcluster C_6 with the ring structure. The van der Waals interaction between the carbon atoms or microclusters and the fullerene surface was approximated by the Lennard–Jones potential $U = 4\varepsilon\left[(\sigma/r^{12}) - (\sigma/r)^6\right]$ with the atomic parameters $\varepsilon = 28$ K and $\sigma = 3.4$ A obtained from graphite compressibility [130]. The interaction between carbon atoms inside C_{60} and C_6 was described by the Born potential

$$U = \frac{\alpha_k - \beta_k}{2} \sum_{i,j=1}^{60} \left[\frac{(\mathbf{u}_i - \mathbf{u}_j)\,\mathbf{r}_{ij}}{|\mathbf{r}_{ij}|}\right]^2 + \frac{\beta_k}{2} \sum_{i,j=1}^{60} (\mathbf{u}_i - \mathbf{u}_j)^2 ,$$

where in the case of C_{60} $k = 1$ for the single bond and $k = 2$ for the double bond, $\mathbf{u}_i$ and $\mathbf{u}_j$ are the displacements of atoms from their equilibrium positions, $\mathbf{r}_i$ are the distances between atoms, and α and β are the force constants. We took $\alpha_1 = \alpha_2 = 1.14 \times 10^6$ dyn cm^{-1} and $\beta_1 = \beta_2 = 1.24 \times 10^5$ dyn cm^{-1}, which were used to calculate the frequencies of internal vibrations in C_{60} [131]. The lengths of single and double bonds in C_{60} were 1.391 and 1.455 A, respectively [132]. The force constants of benzene: $\alpha_6 = 7.62 \times 10^5$ dyn cm^{-1} and $\beta_6 = 0.667 \times 10^5$ dyn cm^{-1} [133] were used for the microcluster C_6. The bond lengths for C_6 were 1.316 A and the angles between them were 90.4° [134]. The calculations were performed for a temperature which was at least 10-fold less than the C_{60}-fullerene melting temperature (many greater than 3000 K [86]), therefore the Born potential was adequate for our simulation. The time integration step was $\rho = 2.5 \times 10^{-15}$ s; the total energy of the system was conserved within the accuracy of 0.5%.

A carbon atom or microcluster was initially positioned at a random place on the C_{60}-fullerene surface. Then the system consisting of fullerene C_{60} and a carbon atom on the fullerene surface relaxed into equilibrium at 40 K over 10^4 steps (approximately 60 atomic oscillations with respect to the surface). Then we heated the system at the rate of 3×10^{-3} K per step until the atom or microcluster desorbed from the surface. Eventually we calculated the average and maximum temperatures of carbon atom desorption, namely, $T_{\mathrm{des}}^{\mathrm{av}} \simeq 120$ K and $T_{\mathrm{des}}^{\mathrm{max}} = 182$ K. The microcluster C_6 turned out to desorb from the fullerene surface at 30 K before the system relaxed into equilibrium.

As was experimentally demonstrated, the transformations of polycyclic hydrocarbons between each other take place only at temperatures higher than 1300 K [111], while amorphous soot transforms into soot with the structure of graphite layers only at temperatures higher than 2500 K [121]. Thus, according to simulation data [127, 128] carbon atoms and microclusters adsorb onto the fullerene surface at a temperature $T < T_{\mathrm{des}}$, which is not explicitly sufficient to rearrange the bonds between the carbon atoms. As a result, a

graphite layer cannot be formed. Therefore, *the shell-by-shell growth of a nanoparticle is impossible in an arc discharge*.

In [127, 128] we simulated only the *physical* adsorption of carbon atoms and microclusters onto the fullerene surface. The calculations of *chemical* adsorption of carbon microclusters do not yield an unambiguous picture of this process. There can be either the insertion of a microcluster into the fullerene structure [135, 92], or the outside localization of carbon atoms chemically bonded to the outer shell. In the first case only the outer shell size increases, while in the second the chemically adsorbed atoms are located twice as close to the shell surface as the next shell coupled with the preceding shell by the van der Waals forces.

According to the shell-by-shell model, the growth of a nanoparticle due to carbon adsorption onto its surface should give rise to nanoparticles with nonclosed external shells. However, they have not been found experimentally, which is an additional argument against the above model.

4.3 Crystallization of a liquid cluster

The following model was proposed for nanoparticle formation. Initially an amorphous viscid cluster arises on the electrode surface and then anneals into a nanoparticle with a shell structure (Fig. 14a) [118]. The model treats the cluster growth as follows. Since the initial cluster extends beyond the electrode surface, the local arc field is greater near the cluster. Hence, the ions, the cluster ions, as well as the atoms and microclusters (because the nonuniform field induces dipole moments in them) are attracted by the arc field to the cluster, leading to its growth.

We propose another way for the formation of a liquid or viscid cluster which is a nanoparticle precursor [127, 128]. The arc discharge between graphite electrodes has two operation modes [136], namely the noisy and quiet states. In the noisy state the graphite electrodes evaporate in the form of atoms and microclusters. This mode corresponds to a greater current density than in the quiet mode [136]. The highest yield of fullerene C_{60} was obtained when the brightness of the arc discharge (consequently, current density) was maximum [136]. Therefore we believe that fullerenes are produced in the noisy mode of arc discharge operation. In the quiet mode, the electrodes evaporate in the form of graphite nanocrystals [136]. On the one hand, nanoparticles and nanotubes are usually produced at a pressure of buffer gas which is several times larger than the optimal for fullerene formation (see, for example, Refs [118, 137]). On the other hand, nanoparticles were obtained in an arc discharge in the absence of a buffer gas [116]. Thus, nanoparticles are produced under conditions different from those for the fullerene production. It is most likely that nanoparticles are formed in the quiet mode of arc discharge operation.

We suppose that nanoparticles arise in an arc discharge from graphite nanocrystals. A temperature of 2500 K is sufficient to transform the structure of carbon nanoparticles [121]. The temperature of the anode spot in an arc discharge between graphite electrodes is 3900 K [136], while the maximum temperature in the plasma amounts to 10000 K [138]. Therefore, there are regions in an arc discharge with temperatures at which evaporated graphite nanocrystals either can transform into shell nanoparticle structures or melt forming nonequilibrium liquid clusters. However, such clusters can leave hot discharge regions before their evaporation. Below we give arguments in favour of this possibility.

Graphite nanocrystals were shown in [136] to be the main positive charge carriers in an arc discharge plasma operating in quiet mode. Typical sizes of graphite nanocrystals are 3 nm [139]. However, nanoparticles with sizes from 10 to 200 nm also arise in an arc discharge [140]. The coagulation of positively charged solid nanoparticles or nanocrystals is highly improbable, because in this case only the electrostatic energy increases. If liquid clusters coagulate, then the increase in the electrostatic energy may be compensated by the decrease in the surface energy. Notice that this mechanism of nanoparticle formation is consistent with the fact that in an arc discharge the nano-particles are found only on the cathode surface [118]. We do not rule out the possibility that liquid carbon clusters are produced in an arc discharge in the

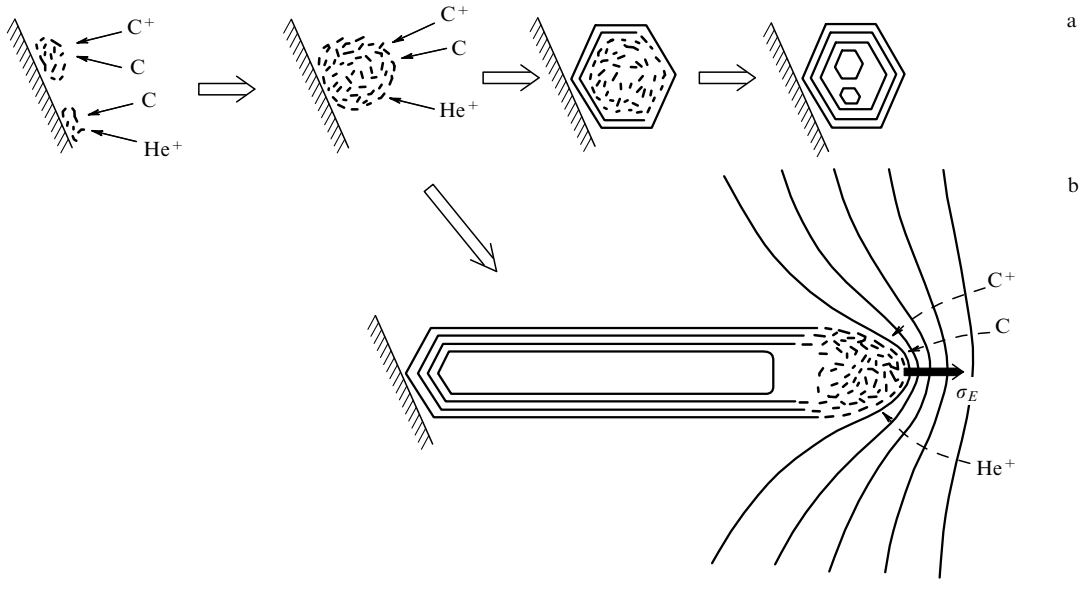

Figure 14. Scheme of formation of a shell nanoparticle (a) and a shell nanotube (b) growing on the electrode surface in an arc discharge [118]. The electric field is indicated by σ_E.

vapor phase. For example, this mechanism of formation in an arc plasma was proposed in [141] for nanoparticles consisting of Fe, Co, or Ni.

Most nanoparticles with shell structures produced in an arc discharge are polyhedra with a cavity in the centre (see, for example, [117, 118]). However, according to the calculations [142], spherical nanoparticles have a lowest binding energy. These calculations are confirmed by experiment, namely, spherical shell nanoparticles can be formed from polyhedra nanoparticles irradiated by electrons [120]. Thus, a liquid carbon cluster crystallizes into the state corresponding to the local energy minimum. To explain this fact, we propose the following scenario for the process [143]. It was assumed [118] that the crystallization of a liquid carbon cluster starts from its surface cooled by buffer gas. We believe that as for fullerene crystallization, a nucleus for shell growth is the cluster C_{20} with a corannulene molecular structure (see Fig. 12). The arguments in favour of this hypothesis were given above in discussing fullerene crystallization. It should be noted also that the structure of each shell includes twelve such elements. The graphite layer may be bent assuming an angular rather than rounded shape to form a stable chain of sp^3 defects [144]. (Carbon atoms in the line of bending are in the sp^3-hybridized state, the angle between the graphite semiplanes depending on the bond angle of these atoms.) In the C_{20} cluster having corannulene molecular structure the atoms are also in the sp^3-hybridized state. Each two atoms corresponding to adjacent sides of the hexagons can be the first atoms of the sp^3-hybridization atomic chain, i.e. the chain of sp^3 defects. Thus, if the cluster with the corannulene molecular structure is a nucleus for the shell growth it may also be a nucleus for the formation of five chains of sp^3 defects with plane graphite sheets between them. In this case, the polyhedron nanoparticle shape may be determined by the energetics of the initial stage of outer shell growth. The formation of the cavity in the nanoparticle centre is explained by the fact that the crystallization of a nanoparticle starts from its surface and the graphite density is greater than the density of liquid or amorphous carbon [118]. The cavity may, possibly, arise not in the centre of the still liquid or amorphous part of the nanoparticle, but near the surface of newly formed shells (i.e. liquid breaks away from the crystal surface). Then, on completing crystallization, a cavity occurs not only in the centre of the nanoparticle but also between the shells. For example, nanoparticles with a shell structure, containing smaller nanoparticles of a similar structure in their cavity, were produced in an arc discharge [145]. The formation of such objects cannot be explained by the shell-by-shell growth of a nanoparticle.

We cannot rule out the possibility that liquid clusters may cool too fast for a shell structure to form. Then amorphous nanoparticles arrive at the electrode and their shell structure and polyhedron shape result from annealing at the hot electrode during the arc discharge [118, 140]. Such annealing was experimentally realized by heating the amorphous soot in the oven [121].

Two types of carbon nanoparticles were found in arc discharges, namely, nanoparticles with a central cavity and those without [140]. The authors of [140] believe that nanoparticles without a cavity arise as a result of shell-by-shell growth. But the resolution of the images of these nanoparticles is not high enough to show their internal structure. Therefore we think that nanoparticles without a cavity have an amorphous structure and are formed on fast freezing of a liquid cluster (see also the consideration for nanoparticles with metal carbide cores below).

Thus, we suppose that the formation of the shell structure during crystallization is universal for carbon clusters of various sizes (one shell for fullerenes and many shells for nanoparticles). Apart from solid carbon clusters there are many other clusters with shell structures. These are, for example, Coulomb clusters [146] confined by an external potential, silicon clusters [147, 148], nanoparticles consisting of boron nitride [149], MoS_2 [150], and WS_2 [151]. The crystallization of a liquid cluster to form a shell structure possibly constitutes a more universal phenomenon taking place for different types of interaction between the particles of the cluster.

Evidently, the number of nanoparticle shells is determined by the number of atoms in a liquid carbon cluster and the conditions its crystallization. According to calculations [152], the nanoparticle C_{300} containing two shells has a greater binding energy than the fullerene C_{300}. Therefore, solid carbon clusters containing several hundreds of atoms, which are usually considered as fullerenes (see, for example, Ref. [29]) may be nanoparticles with two or three shells.

It makes sense to test this assumption by the photodecomposition study of solid carbon clusters containing hundreds of atoms. Both an 'empty' fullerene (see, for example, Refs [90, 77]) and a fullerene with an internal metal atom [153] photodecay with the emission of a C_2 microcluster (since fullerenes have even number of atoms). After disintegration of the fullerene structure, further photodecay of the carbon cluster occurs with the loss of a C_3 microcluster (the microcluster C_3 has a greater binding energy per atom than microcluster C_2 [45]). The situation for the photodecay of a two-shell nanoparticle is similar. As long as the outer shell is large enough to accommodate the inner one, photodecay occurs with the emission of C_2, the outer shell remaining a fullerene. However, the inner shell does not enable the outer one to be decreased freely. Therefore, after the emission of several C_2 microclusters the outer shell is no longer a fullerene, and further photodecay can occur through C_3 emission.

4.4 Formation of nanoparticles with metal or metal carbide cores

In some cases when electrodes contain metals or metal compounds, composite nanoparticles with a metal or metal carbide core covered with carbon also arise in an arc discharge in addition to carbon nanoparticles. Let us discuss the formation of several types of such nanoparticles. Some nanoparticles are polyhedra having a shell structure and a cavity filled (partially, as usual) with a metal crystal or metal carbide crystal. In this case the size of the cavity is comparable with the thickness of the outer carbon shell. For example, when the anode contains ittrium oxides or some lanthanide oxides M_2O_3 (M = Y [154–156], La [156,157], Ce [156, 159], Ho [156, 160] Pr, Nd, Gd, Tb, Dy, Ho, Er, Lu [156]) nanoparticles with a shell structure and a cavity partially filled with MC_2 crystal are formed. According to phase diagrams for the systems Y–C and La–C, graphite, MC_2 (M = Y, La) crystal and a molten mixture with a content of components corresponding to MC_2 are in equilibrium [161]. In Refs [154, 156, 159], a mechanism for the formation of this type of nanoparticles was proposed taking account of this fact. According to this mechanism, a liquid or viscid amorphous cluster is formed initially from metal-carbon

melt, then, as the temperature decreases, graphite crystallizes to form a shell structure on the cluster surface. The carbon crystallization proceeds until the melt composition corresponds to the MC_2 composition, whereupon the melt crystallizes. The process was assumed to take place on the electrode surface [154, 156]. However, amorphous carbon nanoparticles with holmium [156] and cerium [162] carbide cores completely filling a cavity, were also found on the cooled walls of the arc chamber. A liquid or amorphous cluster — the precursor of a nanoparticle — cannot be formed on a cold surface, hence such clusters arise by nucleation from vapor [160], or by melting and aggregation of nanocrystals evaporated from the electrodes. Nanoparticles with holmium carbide cores were detected both in the cathode condensate and on the cooled chamber walls [160]. It turned out that the outer carbon part of the nanoparticles from the chamber walls had an amorphous structure, while that of the nanoparticles from the cathode condensate had a shell structure, the nanoparticles from the cathode condensate also having an unfilled cavity. In our opinion the difference in the nanoparticle structures considered is due to different temperatures on the surfaces where these structures are formed after the precursor cluster was deposited. Notice that if doping of the electrodes by lanthanides does not affect the arc discharge processes, then this is probably also valid for carbon nanoparticles. Moreover, the availability of an unfilled cavity near the core inside the shell nanoparticles, and the lack of such cavity in the amorphous carbon nanoparticles confirm the assumption that purely carbon nanoparticles without a cavity, which are produced in an arc discharge, have an amorphous structure (see above). We believe that other nanoparticles of the same type, for example, nanoparticles with cores of ZrC or V_4C_3 [163] or with crystalline gold cores [164] exhibit a similar formation mechanism.

Nanoparticles of another type have a nearly spherical core 30 – 200 nm in diameter consisting of a metal carbide and covered with several (or several tens) graphite layers which do not form closed shells. For example, nanoparticles were produced with cobalt carbide [141, 165, 156], iron carbide [166, 156], and nickel carbide [156] cores. The carbon film coating the nanoparticle surface was assumed to be formed by release of carbon dissolved in the core [156]. We propose here another possible way of forming the nanoparticles of this type. A spherical metal carbide nanoparticle crystallizes initially from a liquid cluster. Then, metal atoms evaporate from the nanoparticle surface and the remaining carbon atoms form graphite layers. The possibility of such a process was demonstrated in the following experiment: titanium carbide nanocrystals were held at 2200 K. Due to the evaporation of titanium atoms, several graphite layers were formed on the surface of these nanocrystals [167].

A further type of composite nanoparticle produced in an arc discharge are nickel [156, 168], cobalt [165, 156], and iron [166, 156] nanoparticles covered with a thin film of amorphous carbon [156] or graphite layers which do not form closed shells [156, 165, 166, 168]. The formation of these nanoparticles was proposed to be similar to the growth of carbon nanotubes during the catalytic decomposition of hydrocarbons [156] (see the next section). Therefore, we think that the carbon film on these nanoparticles is formed either by the decomposition of metastable carbides existing on the nanoparticle surface or by releasing carbon dissolved in metal.

4.5 Formation of nanoparticle chains

Chains of nanoparticles are found in the cathode condensate when the electrodes contain nickel or its compounds [141, 156, 168], or cobalt [169]. All the nanoparticles have a central cavity, they are very similar in shape and size, and the end nanoparticle usually has a metal core [141, 156]. Two different mechanisms were proposed in Ref. [156] for the formation of chains involving various in form nanoparticles. The formation of chains from roundish particles is explained as follows. All the initial nanoparticles had nickel cores and assemble into a chain due to the interaction between the magnetized cores. Then the temperature increased for some reason in the vicinity of a chain and the nickel evaporated from the nanoparticles, which were not coated completely by carbon film. However, this mechanism does not explain why only the end nanoparticle has a metal core. The other mechanism describes chain formation from oblong nanoparticles. According to this mechanism, carbon dissolves from one side of an oblong nickel core, then it diffuses through the core and condenses at the other core side. The resultant carbon coating escapes periodically from the nanoparticle and forms a nucleus for another nanoparticle in the chain. This mechanism is confirmed by the following experimental fact [156]. Chains of identical oblong nonclosed nanoparticles were detected, the end nanoparticle having an oblong nickel core. The cavity shape in all the nanoparticles coincided with the core shape, while the thickness of the carbon shells increased in the direction of the chain end. The authors of Ref. [141] believe that all the chain nanoparticles are not closed, and have a 'hat-like' shape. Nanoparticles of such a shape can easily escape from the core. Thus, we think that formation of all chains is correctly described by this mechanism. Notice also that it agrees with a possible mechanism for the growth of carbon nanotubes with the help of catalysts (see below).

5. Mechanisms for the growth of nanotubes and cones

This section is devoted to the formation and growth of carbon nanotubes, i.e. filaments with a structure of graphite concentric layers. The main attention is given to new methods of nanotube production in arc discharges and carbon deposition on substrates. While the production of nanotubes and other carbon filaments obtained with the help of catalysts is considered briefly. Mechanisms for the growth of multishell and single-shell nanotubes were analyzed separately. The formation of nanotube bundles and carbon cones is also discussed.

5.1 Growth of multishell nanotubes with the help of catalysts

Carbon nanotubes and filaments have been produced by the catalytic decomposition of hydrocarbons and carbon oxides since the late 1940s (see, for example, the references in [170]). Here we do not dwell upon the growth of nanotubes with the help of catalytic agents, because it was detailed in the review [171]. We only show in outline one of the commonly accepted mechanisms of such growth. A metal nanoparticle is placed at the tip of a growing nanotube. Hydrocarbons are decomposed at one side of this nanoparticle. Carbon diffuses through the nanoparticle or along its surface due to the concentration gradient and forms a nanotube on the other side of the nanoparticle. The carbon at the nanoparticle

surface seems to transform into carbides [172]. This growth mechanism enables carbon to diffuse along the substrate surface as well. In this case nanotubes attach to the substrate by the growing end [174].

The structure of nanotubes and filaments depends on the hydrocarbons and the catalysts used. In particular, filaments consisting of graphite cones inserted one into another [173], nanotubes with outer closed graphite shells and amorphous cores [171] were observed. Sometimes, the shape and diameter of nanotubes and filaments are determined by the shape and diameter of the metal nanoparticles. These nanoobjects produced by catalysis have diameters in the range 10 nm [170] to 5 μm [175]. If a metal particle turns during growth, then curved [170] and spiral-like [176] nanotubes and filaments arise.

5.2 Production and structure of nanotubes

Carbon tubes with graphite layer structures were first obtained in an arc discharge in 1960 [177]. Nevertheless, the size of these objects (5 μm in diameter) does not allow them to be called nanotubes.

Carbon nanotubes were produced at the electrode in an arc discharge by Iijima in 1991 [178] after the discovery of a method for producing macroscopic amounts of fullerenes in an arc discharge [5] (actually nanotubes were observed by Iijima as early as 1980 [179]). Later a technique for producing nanotubes by carbon vapor deposition on a substrate during graphite ablation was reported [180, 181]. Nanotubes were also obtained in flames [182]. Such nanotubes were from 0.6 [183] to 30 nm [178] in diameter and 2 μm in length [181].

Most researchers are of the opinion that nanotubes consist of cylindrical concentric shells. Each shell involves atomic carbon hexagons as in the structure of a graphite layer. In addition to hexagons, the shell structure involves six pentagons at each of the nanotube tip if the shell is closed at this tip. It was also assumed that among cylindrical shells there may be nonclosed spiral shells [184, 185]. As distinct from nanotubes produced (for the most part) by catalysis, the nanotubes fabricated by the above methods are thin and straight. Moreover, single-shell nanotubes were produced by carbon vapor deposition on a substrate (see, for example, Refs [180, 181]) in an arc discharge in the presence of metal (see, for example, Refs [156, 162, 169, 186–184]) and by laser evaporation of a sample containing graphite and metal [195]. Nanotubes produced in an arc discharge [118, 119] or by carbon deposition on a substrate [180, 183] usually grow in bundles.

5.3 Mechanisms for the growth of multishell nanotubes

Several possible mechanisms were proposed for the growth of multishell nanotubes: shell-by-shell growth [97, 116, 117, 140, 184, 197, 198], curling of a graphite sheet [4], and simultaneous growth of all shells [118].

According to the model of shell-by-shell nanotube growth, each next shell results from carbon adsorption onto the surface of the preceding inner shell. Nevertheless, as discussed above on theoretical grounds, carbon atoms and microclusters can adsorb onto the nanoparticle surface only at temperatures less than 200 K [127, 128], which are not sufficient to transform the bonds between carbon atoms, and hence to form the graphite layer of the next nanoparticle shell. Thus, modelling showed that shell-by-shell growth of a nanoparticle as a result of the physical adsorption of carbon atoms or microclusters onto its surface was impossible. The physical adsorption of carbon onto the nanotube surface is analogous to adsorption onto the nanoparticle surface. Therefore, shell-by-shell growth of a nanotube is also very doubtful. In some papers (see, for example, Refs [137, 178]) images of nanotubes with amorphous carbon islands on the surface of the outer shell were published. The advocates of shell-by-shell growth consider these images as an essential argument in favour of this model [197]. However, the *amorphous* structure of these islands confirms the above conclusion that the temperature at which carbon atoms and microclusters adsorb onto the nanotube surface is lower than the temperature at which amorphous carbon possibly rearranges into graphite layers. We suppose that these islands may be formed by the adsorption of carbon atoms and microclusters onto the nanotube surface on switching off the arc discharge and cooling down the electrodes. This assumption does not contradict the simulation data [127, 128], which show that carbon atoms and microclusters adsorb onto the nanoparticle surface only at temperatures less than 200 K. Really, we simulated the adsorption of a microcluster onto the surface of a nanoparticle, which is less curved than the nanoparticle surface with detected amorphous islands. Thus, the average distance between an atom of a microcluster and the nanotube surface is less than the distance used in calculations. Furthermore, all the atoms belonging to the chain-like carbon microcluster can interact with the nanotube surface without bending the chain (as distinct from the interaction with the nanoparticle surface). Therefore, the energy of a carbon microcluster adsorption on the nanotube surface and, hence, the temperature, at which this adsorption is possible, are greater for a nanotube than for a nanoparticle.

Another possibility for shell-by-shell growth is that each shell starts growing from the nanotube base attached to the substrate [97, 184]. In this case the shell can cease growing before it reaches the nanotube tip. However, experiments show that the outer shells of all nanotubes are closed (see, for example, Refs [199, 200]). The only exception are nanotubes produced in an arc discharge in the presence of hydrogen, 3% of which have open shells at the tip [199]. We think that these open shells may result from chemical reactions with hydrogen on completion of the nanotube growth.

It was assumed that nanotubes roll up from a large graphite sheet detached from graphite crystals along the lines of sp^3 defects [4]. However, such a graphite sheet is a parallelogram in shape with an acute angle of 30° [144, 201]. It is impossible to roll up a sheet of such a shape into a nanotube with an equal number of shells along the nanotube length. Scanning tunnelling microscopy did not reveal the sheet edges, which should exist on the nanotube surface with the roll structure [202]. Moreover, different shells of nanotubes were found to have different helicity, or not to be spiral [184]. Such nanotubes cannot roll up from a single graphite sheet. Notice that nanotubes were produced not only during graphite evaporation but also in flames of benzene combustion [182], where the existence of large graphite sheets is very doubtful.

We believe that the remaining possibility is realized and all the nanotube shells grow simultaneously. According to the calculations [203], simultaneous shell growth is energetically preferential. The growth of the nanotube shells in an arc discharge was detailed in Ref. [118]. The nanotube extends beyond the cathode surface, therefore, the arc field is more intense near the nanotube tip. Ions, cluster ions, atoms and microclusters of carbon (since the nonuniform field induces

dipoles in them) are attracted to the growing nanotube tip, but not to the lateral surface. As a result, the nanotubes grow in the direction of the electric field. This oriented nanotube growth is confirmed by experiment (see, for example, Refs [137, 196]).

Nanotubes produced in an arc discharge by using composite electrodes containing graphite and yttrium oxide were observed to be directed perpendicularly to the external surface of metal condensate on the cathode surface [204]. The authors of Ref. [204] use the model of simultaneous shell growth, but they believe that nanotube growth occurs in the direction of the temperature gradient during anode evaporation when the isothermal surface shifts towards the anode.

If all the nanotube shells grow simultaneously, then the growing shells cannot be closed at the end, because carbon has to penetrate through the closed outer shells into the inner ones. However, calculations show that the open shell tip has a lower binding energy than the closed one due to numerous 'dangling' bonds [205]. Several assumptions were made to explain this contradiction. The electric field of an arc discharge was proposed to stabilize the open tip of the nanotube shell [206]. Closing the shells should occur with removing the electric field, but such stabilization of an open nanotube tip is not confirmed by calculations [207, 208]. According to another assumption, there are atoms at the tip of a nanotube which are chemically bonded with two neighbouring shells (Fig. 5) [209]. However, this mechanism of stabilization of the open ends of the shells cannot explain why they close on completion of the nanotube growth. And, finally, one more possibility for nanotube shells to be opened during the growth is as follows: carbon at the growing nanotube tip is in a viscid amorphous state [118], hence it is pointless to speak of growth with the open or closed tip (see Fig. 15). In this case, the shells are closed by crystallization and annealing of the viscid tip after termination of the carbon supply to the tip. A similar growth mechanism with a 'viscid' tip occurs in an arc discharge for multishell nanotubes with yttrium metal core [155]. We suggest that this mechanism also takes place for multishell nanotubes with metal cores consisting of Cr, Ni, Dy, Yb, and Cd [210].

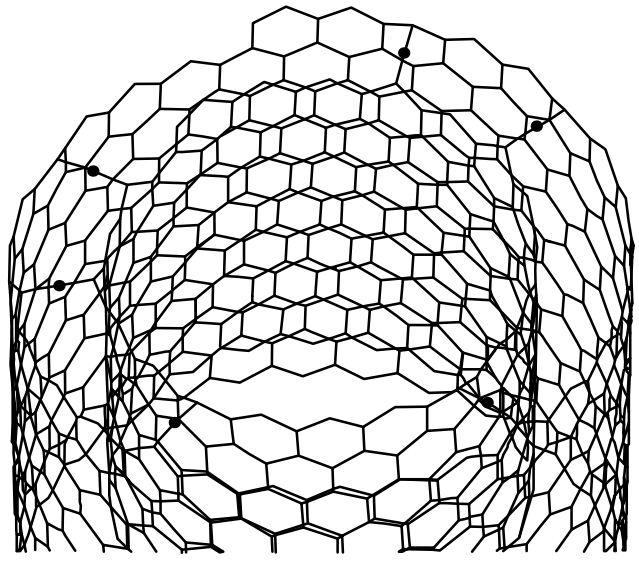

Figure 15. The scheme of a two-shell nanotube with an open tip, where atoms bonding to both the shells are situated [209].

Images of nanotubes with an increased intershell distance were obtained by transmission electron microscopy [211]. It was assumed that some nanotube shells are spiral but not cylindrical [185, 211] (the intershell distance increases in the vicinity of the spiral shell edge). The formation of such a shell was explained by the shell-by-shell model, namely, the opposite sides of a growing shell sometimes overlap but do not join together [185]. We believe that the increased intershell distance at the images corresponds to a real gap between some cylindrical shells. The origin of this gap is analogous to that for the cavity inside a nanoparticle with a shell structure. The annealing of viscid nanotube tip into the shell structure sometimes begins simultaneously for the inmost and outermost shells. As a result, a gap between the shells arises, since the density of carbon with the structure of graphite layers is greater than the density of amorphous carbon.

5.4 Mechanisms for the growth of single-shell nanotubes

Two possible models for the growth of single-shell nanotubes were proposed, namely, growth with an open tip [178, 180, 181, 197, 198] and growth with a closed tip as a result of microcluster insertion into the nanotube structure at its tip [97, 212].

The calculations show that the binding energy for the open tip is less than for the closed one due to numerous 'dangling' bonds [205], and the electric field does not stabilize the growth at the open tip [207, 208]. It is proposed that the electric field induces a charge at the nanotube tip, resulting in a potential barrier which separates the states with closed and open tips [208]. However, single-shell nanotubes were produced also by carbon vapor deposition on a substrate [180, 181], i.e. without an electric field. The growth of a nanotube with an open tip was simulated by molecular dynamics approach in Ref. [213]. A nanotube 1.6 nm in diameter was closed after it joined 18 atoms and further growth occurred with the closed tip.

Microcluster insertion into the fullerene structure was experimentally found by laser desorption [95]. The structure of the closed tip of a single-shell nanotube includes pentagons and hexagons and is similar to that of a fullerene. Thus, insertion takes place only near the pentagons at the nanotube tips, the nanotube length rises only, while its diameter does not change [97, 212]. This possibility is confirmed by the fact [97] that sometimes empty space arises between the outer and inner shells at the nanotube tip. Thus we believe that single-shell nanotubes grow with a closed tip.

5.5 Nuclei for the growth of nanotubes

In two models for the growth of single-shell nanotubes different nuclei were proposed. According to the model for growth of the nanotube with an open tip, the nucleus for the nanotube growth is a cup-like cluster which makes up half of a fullerene [180, 181]. The carbon cluster of this shape has a lot of 'dangling' bonds. Therefore, as is discussed in Section 2, the existence of clusters of such a shape is highly improbable. If it is also assumed that such a cup adsorbs onto the surface [180], then in the case of nanotube growth with an open tip it should be adsorbed by the *inert* part, rather than by the part with *available* bonds, which is not likely either. Another assumption of the model is that a graphite sheet closed in a ring can serve as the nanotube nucleus [198]. Such a cluster has even more 'dangling' bonds than the cup-like cluster, so it can hardly exist as well. According to the model of growth with a closed tip [212], fullerenes are the nuclei for single-shell

nanotube growth. Microcluster insertion into the fullerene structure causes the growth of fullerenes into nanotubes.

Let us discuss the relationship between the shape of large fullerenes consisting of hundreds atoms and mechanisms of nanotube growth. According to the data on scanning tunnelling microscopy [214], all large fullerenes produced in an arc discharge have an almost spherical shape. This shape agrees with the mechanism for fullerene formation by crystallization of a liquid cluster. Notice that large spherical fullerenes have a higher binding energy than oblong fullerenes of the same size [215]. Nevertheless, large fullerenes produced by carbon vapor deposition on a substrate are severely prolate [181]. This shape is consistent with the mechanism for the growth of single-shell nanotubes with closed tips: these oblong fullerenes are very short nanotubes grown from smaller fullerenes due to the insertion of a microcluster into their structure.

It was proposed that carbon nanoparticles are nuclei for the growth of multishell nanotubes in an arc discharge [118]. Fullerenes and small nanoparticles having two or three shells desorb from the electrode surface under arc discharge conditions. For example, the fullerene C_{60}, which can be a nucleus for a growing single-shell nanotube of diameter 0.7 nm, desorbs from the graphite surface at a temperature exceeding 300 K [216]. Therefore, only nanotubes with diameter greater than 2 nm were produced under conditions of arc discharge in the absence of catalysts (see, for example, Refs [137, 200]). On the other hand, nanotubes with diameter less than 1 nm were produced by carbon vapor deposition onto a cold substrate [181].

Many-shell nanotubes are formed not only in an arc discharge but also by vapor deposition of carbon produced by graphite ablation [183]. The possibility of graphite ablation in the nanocrystal form was experimentally examined in Ref. [217]. Therefore, we think that the mechanism for formation of these multishell nanotubes is similar to the mechanism of their formation in an arc discharge, namely, carbon nanoparticles formed from graphite nanocrystals adsorb onto a substrate, where they become nuclei for growing nanotubes, the latter growing with a viscid tip.

Therefore, we believe that nuclei for the growth of single- and multishell nanotubes are *different*, namely, they are fullerenes for single-shell nanotubes and nanoparticles for multishell nanotubes.

5.6 Growth of single-shell nanotubes with the help of catalysts

Single-shell nanotubes grow in an arc discharge only in the presence of metal (see, for example, Refs [156, 162, 169, 186–194]). Single-shell nanotubes were also obtained by laser evaporation of a graphite-metal mixture [195]. The structure and growth mechanisms of single-shell nanotubes produced by these methods depend on the metals or their compounds used as catalysts.

Bundles of short (less than 100 nm) single-shell nanotubes ('sea-urchins') growing on metal carbide nanoparticles were produced in an arc discharge when the anode included yttrium [162, 193] or some other lanthanides such as La [162, 192], Gd, Nd [162, 191], Ce, Tb, Ho, Lu, Er, Pr, or Dy [162]. Experiments on the soot picked up at various distances from the arc show that the bundles of single-shell nanotubes grow on carbon-lanthanum nanoparticles when these nanoparticles are near the arc in the region with temperature 800–1000 K [192]. The authors of Ref. [192] proposed two possible mechanisms for the growth of single-shell nanotubes. According to the first mechanism carbon dissolved in a nanoparticle releases and forms a nanotube as the temperature decreases. In this case nanotube growth takes place on the nanoparticle surface. The second mechanism assumes the growth of a nanotube from the outer tip due to insertion of a carbon atom or microcluster. Similar 'sea-urchin-like' structures were also obtained in [193], but there nanotube bundles and nanoparticle from YC_2 were separated by 10–20 graphite layers and the graphite shell included YC_2 crystal and empty space. It was assumed [193] that initially the nanotubes grew from carbon released from the environmental gas, and then the graphite shell was formed from carbon released from the nanoparticle as the temperature decreased. In this case the graphite structure and the crystal core arise in the nanoparticles due to annealing of an amorphous carbon–metal nanoparticle following the above mechanism (see Section 4.4).

When the evaporating sample includes cobalt [169, 187–189, 195], nickel [156, 188, 195] or their mixture with other metals [188–190, 195] in addition to graphite, a cobweb-like structure arises, which connects 'lumps' of amorphous carbon containing metal nanoparticles. Such a structure is formed either by graphite evaporation in an arc discharge [156, 187–190] or by laser ablation [195]. The threads of the 'cobweb' are isolated single-shell nanotubes [169, 187] or nanotube bundles [187–190]. When the cathode involves iron, and the buffer gas contains methane, a similar structure is formed between cementite nanoparticles [186]. The diameter of nanotubes is usually 1–2 nm, and their length ranges up to 5 μm. A small number of these long single-shell nanotubes is also obtained in an arc discharge when the anode contains iron [188] or platinum [195]. Metal atoms were initially assumed to locate at the nanotube tip and prevent its closure during growth [189]. The distribution of nanotubes over the diameter was found not to be uniform [169]. Since the catalytic activity of a cluster depends on the cluster size, the metal cluster rather than metal atom located at the nanotube tip was assumed [169] to catalyze the nanotube growth. Actually, a nickel cluster of size less than 1 nm was found at the nanotube tip [156]. The assumption that it is cluster that produces a catalytic effect is confirmed by the fact that the use of a mixture of nickel and iron [188], nickel and platinum [195], cobalt and nickel [188, 195], or cobalt and platinum [195] leads to a higher yield of single-shell nanotubes than the use of pure metals. This means that a catalyzer is not a single atom, but a cluster containing atoms of different metals. The amorphous carbon 'lumps' connected together by 'cobweb' of nanothreads usually include metal nanoparticles of size up to 20 nm. However, the nanotube diameter is less than 3 nm (only in the case when sulfur is added to the anode are nanotubes of diameter 6 nm produced). To explain this difference in the sizes of nanotubes and metal nanoparticles, the authors of [195] assumed that the nanotube starts growing from a small metal cluster. The metal atoms attach to the cluster, increasing its size. The attached carbon atoms diffuse to the nanotube origin where they can be inserted individually. This process is more probable than the formation of a nucleus for the next shell or another nanotube of increased diameter, since this formation requires several tens of carbon atoms.

When a copper bar is plugged into the graphite anode, single-shell nanotubes are found in the cathode condensate. The shape of the nanotubes is usually irregular, their diameter

is 1 – 4 nm and length is 3 – 40 nm [194]. The mechanism for the formation of these objects is not yet clear.

5.7 Formation of nanotube bundles

Multi-shell nanotubes produced in an arc discharge (see, for example, Refs [118, 196]) and single-shell nanotubes produced by carbon vapor deposition on a substrate [180] usually grow in bundles. Two assumptions were made to explain this fact. The first is that the close arrangement of nanotube nuclei causes the formation of similar nuclei between them [196]. According to the second assumption, the nanotube nuclei adsorbed onto the substrate form an island [218]. This assumption agrees with the hypotheses that fullerenes and nanoparticles are nuclei for nanotube growth, since these nanoobjects can easily move along the substrate surface and form an island film. Notice that if the cup-like clusters are the nanotube nuclei then they could interact via available bonds in the course of island formation, sticking into fullerenes and nanoparticles.

The structure of nanotubes with alternating regions of single-shell and multishell nanotube was produced by carbon vapor deposition on a substrate [183]. We believe that there were different nuclei for the growth of nanotubes in these regions (fullerenes for single-shell and nanoparticles for multishell nanotubes, respectively). Notice that a nanoparticle domain formed during the deposition of a mixture of fullerenes and nanoparticles was experimentally obtained in Ref. [219], where a mechanism for the formation of an island from nanoparticles was also proposed.

5.8 Formation of carbon cones

In addition to nanotubes, carbon cones were also produced by the carbon vapor deposition on a substrate [220] (Fig. 16). In contrast to the closed nanotube shell including six pentagons at each tip, the cone structure contains five pentagons near the cone tip and seven pentagons near the cone base. It is proposed that the cones grow with an open base, and carbon cup-like clusters containing five pentagons are the nuclei for cone growth [220]. But this model does not explain how the cone base, 8 nm in diameter, is closed by the corresponding 'cap'. We may propose another explanation, namely, these cones grow due to insertion of carbon microclusters into their structure. Microcluster insertion into the structure containing pentagons and heptagons only takes place near the pentagons [97, 212]. Then as for the growth of a single-shell nanotube, the cone structure is reproduced during its growth and the pentagons remain near the cone base and tip. It should be noted that in our model the cone base is initially closed. We believe that asymmetrical fullerenes of a specific shape are the nuclei for cone growth.

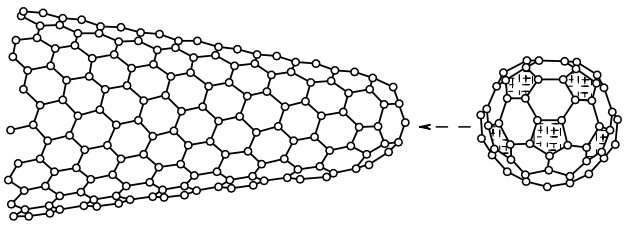

Figure 16. Schematic presentation of the carbon cone tip [220], viewed from the side and from the front. The five pentagons located near the tip of the cone are shaded.

6. Mechanisms for the formation and production of clusters and cluster materials

The above analysis of the mechanisms for the formation of carbon nanostructures allows us to propose some new techniques for producing nanostructures.

6.1 Production of large magic fullerenes

No experimental data have yet been accumulated to conclude which of the fullerenes containing more than 100 atoms are magic. However, it was suggested that such fullerenes may be C_{140}, C_{180} [221], and C_{240} [24, 221]. To produce such great magic fullerenes, one should hold liquid carbon clusters of the corresponding size under the conditions when C_2 emission and insertion reactions in fullerenes occur. In our opinion it is reasonable to combine the experiments on great ordinary and magic fullerenes, namely, to produce great liquid carbon clusters by laser ablation of materials evaporated as carbon clusters containing at least tens of atoms, and then slowly to anneal the mixture of these clusters in an oven filled with inert buffer gas at a temperature of about 1200 K. For example, such materials as finely divided graphite [28], higher oxides of carbon [152], and fullerite [67] may be in use.

6.2 Production of nanoparticles with metal cores

At present there are methods for producing metallofullerenes with several internal metal atoms (see, for example, Ref. [104] and references therein) as well as for carbon nanoparticles with metal cores over 10 nm in diameter (see, for example, Refs [164, 165]). Metal-carbon nanostructures of intermediate size have not been produced so far. We suggest a method to produce nanoparticles with an arbitrary number of metal atoms in the core, and particularly for tens of metal atoms.

For this purpose, in accordance with the above mechanism for the formation of nanoparticles, one should produce liquid metal-carbon clusters containing a certain concentration of metal and constituting a certain size. This can be done as follows. The carbon films have been produced in macroscopic amounts from both single-shell nanotubes in the main [180] and nanotubes 5 μm in diameter [177]. The laser ablation of such films could produce (from nanotube fragments) liquid carbon clusters with a size depending on the nanotube diameter and ablation conditions. The filling of the nanotubes with metal atoms [177] opens up fresh opportunities for the synthesis of metal-carbon nanostructures. We believe that the carbon clusters and nanoparticles with metal cores of various sizes could be produced by laser ablation of metal-filled nanotubes of different diameters. Such nanoobjects may be promising for the development of quantum dot ensembles and new composite materials.

6.3 Production of a crystal from single-shell nanotubes

The bundles of $10^2 - 10^3$ single-shell nanotubes produced by carbon deposition on a substrate were found to be quasi-crystals of nanotubes of the same diameter equal to the diameter of fullerene C_{60} [223]. According to the model for the growth of a single-shell nanotube with a closed tip, the island from fullerenes C_{60} is a nucleus for the growing bundle. We propose using a crystal or film from fullerene C_{60} as a substrate in the nanotube production by the vapor deposition

of carbon. However, the carbon vapor density should be low to prevent fullerene formation. Under such conditions the nanotube nuclei will be identical fullerenes located on the substrate, which will grow into nanotubes by carbon microcluster insertion into their structure. The diameter of each growing nanotube will be equal to that of fullerene C_{60}, while the lattice constant of the nanotube crystal will be equal to that of crystal C_{60}. In this case the number of defects in the nanotube crystal is determined by the number of defects in the initial C_{60} crystal or film.

7. Conclusions

We have analyzed some models for the formation of fullerenes, nanoparticles, nanotubes, and cones.

Theoretical and experimental studies performed so far do not enable us to pitch out one of these mechanisms as the most adequate. But we think that the most probable way for fullerene formation includes the following stages: the formation of liquid carbon clusters; the crystallization of these clusters into fullerenes with the emission of atoms and microclusters; the selection of magic fullerenes via the insertion and emission of C_2 microclusters by fullerenes. This mechanism allows two incongruent facts to be accounted for within one scheme. Firstly, it explains the various sizes and structures of fullerenes formed from hot carbon clusters. Secondly, it reveals the high yield of magic fullerenes with lower rate constants for the reactions of C_2 insertion and emission.

We have considered the mechanisms of selection of fullerene isomers. It is most likely that the main mechanism the reactions of emission and insertion of the C_2 microcluster by fullerenes are as for the selection of magic fullerenes. Another possible way to select isomers is isomer transformations between each other and the different solubility of isomers present in fullerene soot. We propose that the solid carbon clusters produced in an arc discharge or by laser ablation and containing several hundred atoms may have two shells.

We have discussed possible mechanisms for the formation of carbon nanoparticles with shell structures. The model of shell-by-shell growth of a nanoparticle was not confirmed by our molecular dynamics simulation. We suppose that these nanoparticles are formed by liquid cluster crystallization. We have proposed a new mechanism for cluster formation in an arc discharge by the melting of graphite nanocrystals evaporated from electrodes. Mechanisms for the formation of different types of carbon nanoparticles with metal or metal carbide cores have also been analyzed.

We have examined possible mechanisms for the growth of single- and multishell nanotubes. We believe that the experimental and calculated data agree best with the following mechanisms: the single-shell nanotubes grow with a closed tip; all the shells of a multishell nanotube grow simultaneously, and carbon at the tip of a growing nanotube is in an amorphous state. According to these growth mechanisms, fullerenes are the nuclei for the growth of single-shell nanotubes, while nanoparticles are the nuclei for the growth of multishell nanotubes. We suggest a new growth mechanism for carbon cones: they grow with a closed base by C_2 insertion into their structure.

Using the above formation mechanisms, we have proposed some new methods for producing carbon nanoobjects: (1) a method for producing magic fullerenes greater than C_{100}; (2) a method for producing carbon nanoparticles with a metal core of a certain size; (3) a method for producing a crystal from identical single-shell nanotubes by the deposition of carbon on the C_{60}-fullerene film. We believe that experimental investigations of the proposed methods will facilitate the technological progress in the production of carbon nanostructures and serve as a criterion to test the adequacy of the underlying formation mechanisms.

The authors are thankful to L A Chernozatonskiĭ and the A V Eletskiĭ for useful comments. This work was supported by the Russian Foundation for Basic Research, by the programs ''Fullerenes and Atomic Clusters'', ''Surface Atomic Structures'', and ''Physics of Solid-State Structures''. The work by A M Popov was supported by the grant INTAS-93-2492-ext carried out under the research program of International Centre for Fundamental Physics in Moscow.

References

1. Kroto H W et al. *Nature* (London) **318** 162 (1985)
2. Eletskiĭ A V, Smirnov B M *Usp. Fiz. Nauk* **161** (7) 173 (1991) [*Sov. Phys. Usp.* **34** 616 (1991)]
3. Eletskiĭ A V, Smirnov B M *Usp. Fiz. Nauk* **163** (2) 33 (1993) [*Phys. Usp.* **36** 202 (1993)]
4. Eletskiĭ A V, Smirnov B M *Usp. Fiz. Nauk* **165** 977 (1995) [*Phys. Usp.* **38** 935 (1995)]
5. Kratschmer et al. *Nature* (London) **347** 354 (1990)
6. Bochvar D A, Gal'perin E G *Dokl. Akad. Nauk SSSR* **209** 610 (1973)
7. Heath J R et al. *J. Am. Chem. Soc.* **107** 7779 (1985)
8. Parker D H et al. *J. Am. Chem. Soc.* **113** 7499 (1991)
9. Campbell E E et al. *J. Chem. Phys.* **93** 6900 (1990)
10. Brinkmalm G et al. *Chem. Phys. Lett.* **191** 345 (1992)
11. Brown C E et al. *J. Polymer Science* Pt. A **26** 131 (1988)
12. Creasy W R, Brenna J T *Chem. Phys.* **126** 453 (1988)
13. Creasy W R, Brenna J T *J. Chem. Phys.* **92** 2269 (1990)
14. Rubin Y et al. *J. Am. Chem. Soc.* **113** 495 (1991)
15. McElvany S W et al. *Science* **259** 1594 (1993)
16. So H Y, Wilkins C L *J. Phys. Chem.* **93** 1184 (1989)
17. Chem Z Y et al. *Chem. Phys. Lett.*, **198** 118 (1992)
18. Ebreht M et al. *Chem. Phys. Lett.* **214** 34 (1993)
19. Ebreht M et al. *Khim. Fizika* **14** 131 (1995)
20. Howard J B et al. *Nature* (London) **352** 149 (1991)
21. Gerhard P, Loffler S, Homann K H *Chem. Phys. Lett.* **137** 306 (1987)
22. Ebbesen T W, Tabuchi J, Tanigaki K *Chem. Phys. Lett.* **191** 336 (1992)
23. Zhang O L et al. *J. Phys. Chem.* **90** 525 (1986)
24. Kroto H W, McKay K *Nature* (London) **331** 328 (1988)
25. Kroto H W *Science* **242** 1139 (1988)
26. Kroto H W, Allaf A W, Balm S P *Chem. Rev.* **91** 1213 (1991)
27. Curl R F, Smalley R E *Science* **242** 1017 (1988)
28. Yang Y A et al. *Phys. Rev. Lett.* **66** 1205 (1991)
29. Marujama S et al. *Z. Phys. D* **19** 409 (1991)
30. Baum R M *Chem. and Eng. News* **68** 30 (1990)
31. Ebert L B *Science* **247** 1468 (1989)
32. Curl R F, Smalley R E *Sci. Am.* **265** 55 (1991)
33. Haufler R E et al. *Mat. Res. Soc. Proc.* **206** 627 (1991)
34. Rohlfing E A, Cox D M, Kaldor A *J. Chem. Phys.* **81** 3322 (1984)
35. Smalley R E *Acc. Chem. Res.* **25** 98 (1992)
36. Chang T M et al. *J. Am. Chem. Soc.* **114** 7603 (1992)
37. Goeves A, Sedlmayer E *Chem. Phys. Lett.* **184** 310 (1991)
38. Wakabayachi T, Achiba Y *Chem. Phys. Lett.* **190** 465 (1992)
39. Achiba Y et al., in *Proc. First Workshop on Fullerenes: Status and Perspectives* (Eds C Taliani, G Ruani, R Zamboni) (Bologna, Italy, Feb. 6–7, 1992) p. 13
40. Wakabayachi et al. *Chem. Phys. Lett.* **201** 471 (1993)
41. Dias J R *Chem. Phys. Lett.* **209** 439 (1993)
42. Kikuchi K et al. *Nature* (London) **357** 142 (1992)
43. Scheider U et al. *Chem. Phys. Lett.* **210** 165 (1993)

44. Tomanek D, Schluter M A *Phys. Rev. Lett.* **67** 2331 (1991)
45. Raghavachari K, Binkley J S *J. Chem. Phys.* **87** 2191 (1987)
46. Andreoni W, Scharf D, Giannozzi P *Chem. Phys. Lett.* **173** 449 (1990)
47. Zerbetto F *Chem. Phys.* **150** 39 (1991)
48. von Helden G et al. *Science* **259** 1300 (1993)
49. von Helden G et al. *J. Chem. Phys.* **95** 3835 (1991)
50. von Helden G et al. *J. Phys. Chem.* **97** 8182 (1993)
51. von Helden G et al. *Chem. Phys. Lett.* **204** 15 (1993)
52. Yang S et al. *Chem. Phys. Lett.* **144** 431 (1988)
53. Broyer M et al. *Chem. Phys. Lett.* **198** 128 (1992)
54. Rohlfing E A *J. Chem. Phys.* **93** 7851 (1990)
55. Jing X, Chelikowsky J R *Phys. Rev. B* **46** 5028 (1992)
56. Pope C J, Harr J A, Howard J B *J. Phys. Chem.* **97** 11001 (1993)
57. Taylor R et al. *Nature* (London) **366** 728 (1993)
58. Heath J R, in *Fullerenes: Synthesis, Properties and Chemistry of Large Carbon Clusters* (Eds G S I Hammond, V J Kuck) pp. 1 – 23 (Washington, DC: American Chemical Society, 1991)
59. Lozovik Yu E, Popov A M *Phys. Low-Dim. Struct.* **6** 33 (1994)
60. Sawtarie M, Menon M, Subbaswamy K R *Phys. Rev. B* **49** 7739 (1994)
61. Brabec C J et al. *Phys. Rev. B* **46** 7326 (1992)
62. von Helden G, Gotts N G, Bowers M T *Nature* (London) **363** 60 (1993)
63. Hunter J, Fue J, Jarrold M F *J. Phys. Chem.* **97** 3460 (1993); *J. Chem. Phys.* **99** 1785 (1993); *Science* **260** 784 (1993)
64. Astakhova T Yu, Shaginyan Sh A, Vinogradov G A, in *Proc. of MRS Symposium* (Boston, USA, 1994)
65. Vinogradov G A, Astakhova T Yu, Shaginyan Sh A, in *Proc. Int. Workshop on Fullerenes and Atomic Clusters, Abstracts of Invited Lectures and Contributed Papers* (St. Petersburg, Russia, 19 – 24 June 1995) p. 43
66. Astakhova T Yu et al. *Khim. Fizika* **15** (10) 39 (1996)
67. Yeretzian C et al. *Nature* (London) **359** 44 (1992)
68. Chai Y et al. *J. Phys. Chem.* **95** 7564 (1991)
69. Jin C et al., in *Proc. First Workshop on Fullerenes: Status and Perspectives* (Eds C Taliani, G Ruani, R Zamboni) (Bologna, Italy, Feb. 6 – 7, 1992) p. 21
70. Strout D L et al *J. Phys. Chem.* **98** 8622 (1994)
71. Strout D L, Scuseria G E *J. Phys. Chem.* **100** 6492 (1996)
72. Creasy W R *J. Chem. Phys.* **92** 7223 (1990)
73. Shaginyan Sh A et al., in *Proc. Int. Workshop on Fullerenes and Atomic Clusters, Abstracts of Invited Lectures and Contributed Papers* (St. Petersburg, Russia, 19 – 24 June 1995) p. 151
74. Schweigert V A et al. *Chem. Phys. Lett.* **235** 221 (1995)
75. Hawkins J M *J. Am. Chem. Soc.* **113** 9394 (1991)
76. Yannoni C S et al. *J. Am. Chem. Soc.* **113** 3190 (1992)
77. Radi P P et al. *J. Chem. Phys.* **88** 2809 (1988)
78. Nerushev O A, Sukhinin G I *Pis'ma Zh. Tekh. Fiz.* **21** (13) 50 (1995) [*Tech. Phys. Lett.* **21** 514 (1995)]
79. Saito S, Sawada S *Chem. Phys. Lett.* **198** 466 (1992)
80. Sanders M et al. *Nature* (London) **367** 256 (1994)
81. Murry R L, Scuceria G E *Science* **263** 791 (1994)
82. Astakhova T Yu, Shaginyan Sh A, Vinogradov G A, in *Proc. Int. Workshop on Fullerenes and Atomic Clusters, Abstracts of Invited Lectures and Contributed Papers* (St. Petersburg, Russia, 19 – 24 June 1995) p. 80
83. Terrones H *Ful. Sc. Tech.* **3** 107 (1995)
84. Chelikowsky J R *Phys. Rev. Lett.* **67** 2970 (1992)
85. Wang C Z et al. *J. Phys. Chem.* **96** 3563 (1992)
86. Chelikowsky J R *Phys. Rev. B* **45** 12062 (1992)
87. Guo T et al. *Science* **257** 1661 (1992)
88. Hahn H Y et al. *Chem. Phys. Lett.* **130** 12 (1987)
89. Diederich A F et al. *Science* **252** 548 (1991)
90. O'Brien S C et al. *J. Chem. Phys.* **88** 220 (1988)
91. Lykke K R, Wurz P *J. Phys. Chem.* **96** 3191 (1992)
92. Yi J Y, Bernhole J *Phys. Rev. B* **48** 5724 (1993)
93. Kasuya K, Nishina Y *Z. Phys. D* **12** 493 (1989)
94. JANAF Thermochemical Tables, 2nd ed., NSRDS-NBS 37 (Washington: Nat. Bur. Stand., 1970)
95. Ulmer G et al. *Chem. Phys. Lett.* **182** 114 (1991)
96. Kikuchi K et al. *Chem. Phys. Lett.* **188** 177 (1992)
97. Endo M, Kroto H W *J. Phys. Chem.* **96** 6941 (1992)
98. Curl R F *Phil. Trans. R. Soc. Lond. A* **343** 19 (1993)
99. Campbell E E et al. *Chem. Phys. Lett.* **175** 505 (1990)
100. Radi P P et al. *Chem. Phys. Lett.* **174** 223 (1990)
101. Bunchah R F et al. *J. Chem. Phys.* **96** 6866 (1992)
102. Aced G et al., in *Proc. Int. Winterschool on Electronic Properties of Novel Materials: Progress in Fullerenes Research* (Tyrol, Austria, 5 – 12 March 1994) p. 74
103. Tohji K et al. *J. Phys. Chem.* **99** 17785 (1995)
104. Bethune D S et al. *Nature* (London) **366** 123 (1993)
105. Kroto H W *Nature* (London) **329** 529 (1987)
106. Zhang B L, Wang C Z, Ho K M *Chem. Phys. Lett.* **193** 225 (1992)
107. Stone A J, Wales D J *Chem. Phys. Lett.* **128** 501 (1986)
108. Murry R L et al. *Nature* (London) **366** 665 (1993)
109. Eggen B R et al. *Science* **272** 87 (1996)
110. Mintmire J W *Science* **272** 45 (1996)
111. Scott L T, Roelofs N H *J. Am. Chem. Soc.* **109** 5461 (1987)
112. Adams G B et al. *Chem. Phys.* **176** 61 (1993)
113. Afanas'ev D et al. *Zh. Tekh. Fiz.* **64** 76 (1994)
114. Saito Y et al. *Chem. Phys. Lett.* **200** 643 (1993)
115. Fiber-Erdmann M et al., in *Proc. Int. Winterschool on Electronic Properties of Novel Materials: Progress in Fullerenes Research* (Tyrol, Austria, 5 – 12 March 1994) p. 62
116. Ugarte D *Chem. Phys. Lett.* **198** 596 (1992)
117. Ajayan P M, Ichihashi T, Iijima S *Chem. Phys. Lett.* **202** 384 (1993)
118. Saito Y et al. *Chem. Phys. Lett.* **204** 277 (1993)
119. Ugarte D *Nature* (London) **359** 707 (1992)
120. Ugarte D *Chem. Phys. Lett.* **207** 473 (1993)
121. Heer W A, Ugarte D *Chem. Phys. Lett.* **207** 480 (1993)
122. Kuznetsov V L et al. *Chem. Phys. Lett.* **222** 344 (1994)
123. Kovalevskii V V, in *Proc. Int. Workshop on Fullerenes and Atomic Clusters, Abstracts of Invited Lectures and Contributed Papers* (St. Petersburg, Russia, 19 – 24 June 1995) p. 67
124. Iijima S *J. Crystal Growth* **50** 675 (1980)
125. Tarnai T *Phil. Trans. R. Soc. Lond. A* **343** 145 (1993)
126. Yamada K, Kunishige H, Sawaoka A B *Naturwissenschaften* **78** 450 (1991)
127. Lozovik Yu E, Popov A M *Phys. Lett. A* **189** 127 (1994)
128. Lozovik Yu E, Popov A M *Teplofiz. Vys. Temp.* **33** 534 (1995)
129. Iijima S *J. Phys. Chem.* **91** 3466 (1987)
130. Cheng A, Klein M L *J. Phys. Chem.* **95** 6750 (1991)
131. Jiang Q et al. *Chem. Phys. Lett.* **191** 197 (1992)
132. David W I F et al. *Nature* (London) **353** 147 (1991)
133. Crawford B L, Miller F A *J. Chem. Phys.* **17** 249 (1949)
134. Raghavachari K *Z. Phys. D* **12** 61 (1989)
135. Murry R L et al. *Nature* (London) **366** 665 (1993)
136. Abrahamson J *Carbon* **12** 111 (1974)
137. Ebbesen T W, Ajayan P M *Nature* (London) **358** 220 (1992)
138. Chibante L P F et al. *J. Phys. Chem.* **97** 8694 (1993)
139. Abrahamson J *Carbon* **11** 337 (1973)
140. Koprinapov N et al. *J. Phys. Chem.* **99** 2042 (1995)
141. Yosida Y et al. *J. Appl. Phys.* **76** 4533 (1994)
142. Lu J P, Yang W *Phys. Rev. B* **46** 11421 (1992)
143. Lozovik Yu E, Popov A M *Phys. Low-Dim. Struct.* **12** 173 (1995)
144. Huira H et al. *Nature* (London) **367** 148 (1994)
145. Dravid V P et al. *Science* **259** 1601 (1993)
146. Lozovik Yu E *Usp. Fiz. Nauk* **153** 356 (1987) [*Sov. Phys. Usp.* **30** 912 (1987)]; Lozovik Yu E, Mandelstam V A *Phys. Lett. A* **145** 269 (1990)
147. Rothlisberger U, Andreoni W, Parinello M *Phys. Rev. Lett.* **72** 665 (1994)
148. Pan J, Ramakrishna M V *Phys. Rev. B* **50** 15431 (1994)
149. Boulanger L et al. *Chem. Phys. Lett.* **234** 227 (1995)
150. Margulis L et al. *Nature* (London) **365** 113 (1993)
151. Tenne R et al. *Nature* (London) **360** 444 (1992)
152. Maiti A, Brabec C J, Bernhole J *Phys. Rev. Lett.* **70** 3023 (1993)
153. Weiss F D et al. *J. Am. Chem. Soc.* **110** 4464 (1988)
154. Saito Y et al. *Chem. Phys. Lett.* **209** 72 (1993)
155. Seraphin S et al. *Appl. Phys. Lett.* **63** 2073 (1993)
156. Saito Y et al. *J. Phys. Chem. Solids* **54** 1849 (1993)
157. Ruoff R S et al. *Science* **259** 346 (1993)
158. Tonita M, Saito Y, Hayashi T *Jpn. J. Appl. Phys., Part* **2** 32 L280 (1993)
159. Yosida Y *Appl. Phys. Lett.* **62** 3447 (1993)

160. Scott J H J, Majetich S A *Phys. Rev. B* **52** 12564 (1995)
161. Gschneider K A, Calderwood F W, in *Binary Alloy Phase Diagrams* Vol. 1 (Eds T B Massalshi et al.) (ASM International, Materials Park, 1990) p. 895
162. Saito Y, Kawabata K, Okuda M *J. Phys. Chem.* **99** 16076 (1995)
163. Bandow S, Saito Y *Jpn. J. Appl. Phys.* **32** L1677 (1993)
164. Ugarte D *Chem. Phys. Lett.* **209** 99 (1993)
165. Saito Y et al. *J. Appl. Phys.* **75** 134 (1994)
166. Saito Y et al. *Chem. Phys. Lett.* **212** 379 (1993)
167. Suzuki T et al. *J. Appl. Phys.* **77** 3450 (1995)
168. Seraphin S et al. *Chem. Phys. Lett.* **217** 191 (1994)
169. Kiang C H et al. *J. Phys. Chem.* **98** 6612 (1994)
170. Baker R T K et al. *J. Catalysis* **26** 51 (1972)
171. Baker R T K *Carbon* **27** 315 (1989)
172. Alstrup I *J. Catalysis* **109** 241 (1988)
173. Kock A J H M et al. *J. Catalysis* **96** 481 (1985)
174. Amelinckx S et al. *Science* **265** 635 (1994)
175. McAllister P, Wolf E E *Carbon* **30** 189 (1992)
176. Ruston W R et al. *Carbon* **7** 47 (1969)
177. Bacon R *J. Appl. Phys.* **31** 283 (1960)
178. Iijima S *Nature* **354** 56 (1991)
179. Iijima S *J. Microscopy* **119** 99 (1980)
180. Kosakovskaya Z Ya, Chernozatonskiĭ L A, Fedorov E A *Pis'ma Zh. Eksp. Teor. Fiz.* **56** 26 (1992) [*JETP Lett.* **56** 26 (1992)]
181. Ge M, Sattler K *Science* **260** 515 (1993)
182. Duan H M, McKinnon J T *J. Phys. Chem.* **98** 12815 (1994)
183. Chernozatonskii L A et al. *Phys. Lett. A* **197** 40 (1995)
184. Zhang X P et al *J. Crystal Growth* **130** 368 (1993)
185. Amelinckx S et al. *Science* **267** 1334 (1995)
186. Iijima S, Ichihashi T *Nature* (London) **363** 603 (1993)
187. Bentune D S et al. *Nature* (London) **363** 605 (1993)
188. Seraphin S, Zhou D *Appl. Phys. Lett.* **64** 2087 (1994)
189. Ajayan P M et al. *Chem. Phys. Lett.* **215** 509 (1993)
190. Lambert J M et al. *Chem. Phys. Lett.* **226** 364 (1994)
191. Subramoney S et al. *Nature* (London) **366** 637 (1993)
192. Saito Y et al. *Chem. Phys. Lett.* **236** 419 (1995)
193. Zhou D, Seraphin S, Wang S *Appl. Phys. Lett.* **65** 1593 (1994)
194. Lin X et al. *Appl. Phys. Lett.* **64** 181 (1994)
195. Guo T et al. *Chem. Phys. Lett.* **243** 49 (1995)
196. Ebbesen T W et al. *Chem. Phys. Lett.* **209** 83 (1993)
197. Iijima S, Ajayan P M, Ichihashi T *Phys. Rev. Lett.* **69** 3100 (1992)
198. Hatta N, Murata K *Chem. Phys. Lett.* **217** 398 (1994)
199. Wang X K et al. *Appl. Phys. Lett.* **66** 2430 (1995)
200. Gallghen M T et al. *Surf. Sc. Lett.* **281** L335 (1993)
201. Ebbesen T W, in *Proc. Int. Winterschool on Electronic Properties of Novel Materials: Progress in Fullerenes Research* (Tyrol, Austria, 5–12 March 1994) p. 116
202. Ge M, Sattler K *J. Phys. Chem. Solids* **54** 1871 (1993)
203. Tibbetts G G *J. Crystal Growth* **66** 632 (1984)
204. Shi Z et al. *Solid State Commun.* **97** 371 (1996)
205. Rotkin V V, Suris R A, in *Proc. Int. Workshop on Fullerenes and Atomic Clusters, Abstracts of Invited Lectures and Contributed Papers* (St. Petersburg, Russia, 19–24 June 1995) p. 25
206. Smalley R E *Mater. Sci. Eng. B* **19** 1 (1993)
207. Maiti A et al. *Phys. Rev. Lett.* **73** 2468 (1994)
208. Nordlander P, Lou L P, Smalley R E *Phys. Rev. B* **52** 1429 (1995)
209. Guo T et al. *J. Phys. Chem.* **99** 10694 (1995)
210. Guervet-Plecout C et al. *Nature* (London) **372** 762 (1994)
211. Li Z G, Fagan P J, Liang L *Chem. Phys. Lett.* **207** 148 (1993)
212. Saito Y, Dresselhaus G, Dresselhaus M S *Chem. Phys. Lett.* **195** 537 (1992)
213. Maiti A et al. *Chem. Phys. Lett.* **236** 150 (1995)
214. Lamb L D et al. *Science* **255** 1413 (1992)
215. Adams G B et al. *Science* **256** 1792 (1992)
216. Ruoff R S, Hickman A P *J. Phys. Chem.* **97** 2492 (1993)
217. Rohlfing E A *J. Chem. Phys.* **89** 6103 (1988)
218. Kosakovskaja Z Ya, in *Proc. Int. Workshop on Fullerenes and Atomic Clusters, Abstracts of Invited Lectures and Contributed Papers* (St. Petersburg, Russia, 19–24 June 1995) p. 19
219. Molchanov S P, Popov A M, Sukhorukov A V *Poverkhnost'* **8–9** 42 (1994)
220. Ge M, Sattler K *Chem. Phys. Lett.* **220** 192 (1994)
221. Klein D J, Seitz W A, Schmalz T G *Nature* (London) **323** 703 (1986)
222. Ajayan P M, Iijima S *Nature* (London) **361** 123 (1992)
223. Omel'yanovskiĭ O E et al. *Pis'ma Zh. Eksp. Teor. Fiz.* **62** 503 (1995) [*JETP Lett.* **62** 483 (1995)]